A Well-Balanced Asymptotic Preserving Scheme for the Two-Dimensional Rotating Shallow Water Equations with Nonflat Bottom Topography

Alexander Kurganov*, Yongle Liu† and Mária Lukáčová-Medviďová‡

Abstract

We consider the two-dimensional rotating shallow water equations with nonflat bottom topography. We focus on the case of low Froude number, in which the system is stiff and conventional explicit numerical methods are extremely inefficient and often impractical. Our goal is to design a finite volume scheme, which is both asymptotic preserving (uniformly asymptotically consistent and stable for a broad range of low Froude numbers) and well-balanced (capable of exactly preserving geophysically relevant steady-state solutions). The goal is achieved in two steps. We first rewrite the studied equations in terms of perturbations of the steady state and then apply the flux splitting similar to the one used in [Liu *et al.*, J. Comput. Phys., 391 (2019), pp. 259–279]. We split the flux into the stiff and nonstiff parts and then use an implicit-explicit approach: apply an explicit second-order central-upwind scheme to the nonstiff part of the system while treating the stiff part implicitly. As the stiff part of the flux is linear, we reduce the implicit stage of the proposed method to solving a Poisson-type elliptic equation, which is discretized using a standard second-order central difference scheme.

We prove the asymptotic preserving property of the developed scheme and conduct a series of numerical experiments, which demonstrate that our scheme outperforms the non-well-balanced asymptotic preserving scheme from [Liu *et al.*, J. Comput. Phys., 391 (2019), pp. 259–279].

Key words: rotating shallow water equations, asymptotic preserving scheme, well-balanced scheme, central-upwind scheme, flux splitting, implicit-explicit approach.

AMS subject classification: 76M12, 65M08, 35L65, 86-08, 65M99

*Department of Mathematics, SUSTech International Center for Mathematics and Guangdong Provincial Key Laboratory of Computational Science and Material Design, Southern University of Science and Technology, Shenzhen, 518055, China; alexander@sustech.edu.cn

†Department of Mathematics, Harbin Institute of Technology, Harbin, 150001, China and Department of Mathematics, Southern University of Science and Technology, Shenzhen, 518055, China; liuyl2017@mail.sustech.edu.cn

‡Institute of Mathematics, University of Mainz, Germany; lukacova@uni-mainz.de

1 Introduction

Rotating shallow water (RSW) equations are often used to model oceanic and atmospheric circulations; see, e.g., [11, 21, 34, 37–39, 41, 46]. In the case of the nonflat bottom topography, the two-dimensional RSW equations read as

$$\begin{aligned} &h_t + (hu)_x + (hv)_y = 0,\\ &(hu)_t + \Big(hu^2 + g\frac{h^2}{2}\Big)_x + (huv)_y = fhv - ghZ_x,\\ &(hv)_t + (huv)_x + \Big(hv^2 + g\frac{h^2}{2}\Big)_y = -fhu - ghZ_y, \end{aligned} \tag{1.1}$$

where t is time, x and y are horizontal spatial coordinates, $h(x,y,t)$ is the water depth, $u(x,y,t)$ and $v(x,y,t)$ are the x- and y-components of the flow velocity, g is the constant gravitational acceleration, f is the Coriolis parameter, and $Z(x,y)$ is the bottom topography.

The RSW system (1.1) is a nonlinear hyperbolic system of balance laws. Their solutions may develop a complex wave structure including nonlinear shock and rarefaction waves, as well as linear contact waves. Therefore, solving (1.1) numerically requires development of shock-capturing methods, which utilize nonlinear mechanisms to stabilize computed solutions; see, e.g., [7,16,23,30] and references therein.

Moreover, the RSW equations admit nontrivial steady-state solutions (equilibria). In fact, many geophysical flows are small perturbations of the so-called geostrophic equilibria satisfying

$$u_x + v_y = 0, \quad g(h+Z)_x = fv, \quad g(h+Z)_y = -fu. \tag{1.2}$$

Therefore, one needs to develop well-balanced (WB) shock-capturing schemes, which are capable of exactly preserving geostrophic steady states and thus accurately capture their small perturbations on (computationally affordable) coarse grids; see, e.g., [2, 3, 6, 8, 22, 33].

In [9], the authors proposed two WB second-order finite volume methods that are capable of exactly preserving some of the geostrophic steady states satisfying (1.2) and accurately capturing their small perturbations. However, the WB methods developed in [9] did not take into account a multiscale character of typical oceanic and atmospheric flows. Consequently, these methods were inefficient in geophysically relevant low Froude number regimes. For instance, the current velocity in oceans is approximately $u_{\rm char} = 1$ m/s and the vertical length depth $h_{\rm char}$ is around $100 - 1000$ m. This means that typical advection speed $u_{\rm char}$ is much smaller then the speed of gravitational waves $c_{\rm char} = \sqrt{gh_{\rm char}}$, and thus the Froude number ${\rm Fr} := u_{\rm char}/c_{\rm char} \ll 1$ (typically being in the range $0.01 - 0.032$). The latter implies that there are terms of a very different magnitudes in (1.1) and hence, if an explicit time discretization of (1.1) is used, the CFL stability condition may impose severe restrictions on the size of time steps. Moreover, the size of the spatial grid required to be used to ensure that the amount of numerical diffusion is not unphysically large, must be also taken sufficiently fine and the resulting numerical method may become impractically inefficient.

The multiscale character of a studied problem can be taken into account in the framework of the so-called *asymptotic preserving (AP)* methods; see, e.g., [18, 19], where the concept of AP methods was introduced. A numerical scheme is called AP if it is uniformly consistent and stable as a singular perturbation parameter, for instance the Froude number, approaches its limit, that is, ${\rm Fr} \to 0$. In particular, the AP scheme should reduce to a consistent approximation of the limiting equations as ${\rm Fr} \to 0$ and the stability time-step restriction should be independent of Fr.

The AP schemes have been widely studied for the kinetic equations; see, e.g., [17, 20] and references therein. They have been also applied to the low Mach number compressible Euler and Navier-Stokes equations in, e.g., [5, 10, 12, 14, 36, 45]. Several AP schemes were developed for the Saint-Venant system of shallow water equations; see e.g., [4, 13, 43]. Adding Coriolis forces to the Saint-Venant system brings another level of complexity since in the RSW equations, not only the hydrostatic pressure, but also the Coriolis term is stiff in the low Froude number regime. An asymptotically consistent method for the RSW equations was developed in [44] and an AP scheme has been recently developed in [32].

The goal of this paper is to design a new finite volume method for the RSW system (1.1) that is both WB and AP. To this end, we will first rewrite the RSW system (1.1) in terms of a perturbation of the geostrophic steady state. The rewritten system will be discretized using the stiff-nonstiff flux splitting approach from [14, 32] and an implicit-explicit time discretization. The nonstiff part of the flux will be approximated using the central-upwind (CU) numerical flux. The CU finite volume schemes were developed in [24, 25, 27, 28] as a class of simple (Riemann-problem-solver-free), efficient and highly accurate "black-box" solvers for multidimensional hyperbolic systems of conservation laws. The CU schemes were extended to the hyperbolic systems of balance laws and, in particular, to a variety of shallow water models; see [23] and references therein. CU schemes were also applied to the RSW equations (1.1): a WB CU scheme was proposed in [9], while an AP CU scheme was introduced in [32].

The present paper is organized as follows. Section 2 is devoted to a nondimensional reformulation of the RSW system (1.1) and its asymptotic analysis. In Section 3, we develop and analyze a new WB-AP CU scheme. Finally, in Section 4, we test our new WB-AP CU scheme on a number of numerical experiments.

2 Nondimensional Reformulation of the RSW Equations

We begin with the derivation of a nondimensional form of the RSW equations (1.1). To this end, we first introduce the following characteristic scales: t_{char} is the characteristic time, L_{char} is the characteristic length, H_{char} is the characteristic depth, and u_{char} the the characteristic velocity. We then rescale (1.1) and obtain the nondimensional form of the RSW equations:

$$\begin{aligned}
&\mathrm{Sr}\cdot h_t+(hu)_x+(hv)_y=0,\\
&\mathrm{Sr}\cdot (hu)_t+\left(hu^2+\frac{1}{\mathrm{Fr}^2}\frac{h^2}{2}\right)_x+(huv)_y=\frac{1}{\mathrm{Ro}}hv-\frac{1}{\mathrm{Fr}^2}hZ_x,\\
&\mathrm{Sr}\cdot (hv)_t+(huv)_x+\left(hv^2+\frac{1}{\mathrm{Fr}^2}\frac{h^2}{2}\right)_y=-\frac{1}{\mathrm{Ro}}hu-\frac{1}{\mathrm{Fr}^2}hZ_y,
\end{aligned}\tag{2.1}$$

where

$$\mathrm{Sr}:=\frac{L_{\text{char}}}{t_{\text{char}}u_{\text{char}}},\quad \mathrm{Fr}:=\frac{u_{\text{char}}}{\sqrt{gH_{\text{char}}}},\quad \mathrm{Ro}:=\frac{u_{\text{char}}}{L_{\text{char}}f},$$

are the Strouhal, Froude and Rossby numbers, respectively. Choosing $t_{\text{char}}=L_{\text{char}}/u_{\text{char}}$ and $H_{\text{char}}=L^2_{\text{char}}/g$ and denoting the reference Froude number by $\mathrm{Fr}=:\varepsilon$, we obtain $\mathrm{Sr}=1$, $\mathrm{Ro}=\varepsilon$,

and rewrite the system (2.1) as

$$\begin{cases} h_t + (hu)_x + (hv)_y = 0, \\ (hu)_t + (hu^2)_x + (huv)_y + \dfrac{1}{\varepsilon^2}\left(\dfrac{h^2}{2}\right)_x = \dfrac{1}{\varepsilon}hv - \dfrac{1}{\varepsilon^2}hZ_x, \\ (hv)_t + (huv)_x + (hv^2)_y + \dfrac{1}{\varepsilon^2}\left(\dfrac{h^2}{2}\right)_y = -\dfrac{1}{\varepsilon}hu - \dfrac{1}{\varepsilon^2}hZ_y. \end{cases} \tag{2.2}$$

The formulation (2.2) clearly points out the multiscale character of the RSW model (1.1) and identifies the terms of different ε-orders.

Let us now consider a steady-state solution denoted by $\hat{h}$, $\hat{u}$ and $\hat{v}$, that is,

$$(\hat{h}\hat{u})_x + (\hat{h}\hat{v})_y = 0, \tag{2.3a}$$

$$(\hat{h}\hat{u}^2)_x + (\hat{h}\hat{u}\hat{v})_y + \frac{1}{\varepsilon^2}\hat{h}\hat{h}_x = \frac{1}{\varepsilon}\hat{h}\hat{v} - \frac{1}{\varepsilon^2}\hat{h}Z_x, \tag{2.3b}$$

$$(\hat{h}\hat{u}\hat{v})_x + (\hat{h}\hat{v}^2)_y + \frac{1}{\varepsilon^2}\hat{h}\hat{h}_y = -\frac{1}{\varepsilon}\hat{h}\hat{u} - \frac{1}{\varepsilon^2}\hat{h}Z_y. \tag{2.3c}$$

Moreover, any solution (h, u, v) of (2.2) can be written as

$$h = \hat{h} + h', \quad u = \hat{u} + u', \quad v = \hat{v} + v', \tag{2.4}$$

where h', u' and v' are the perturbations of the equilibrium $(\hat{h}, \hat{u}, \hat{v})$. In what follows we assume that the steady state is given and rewrite the system (2.2) by using (2.3) and (2.4). This results in the following reformulation of the original RSW equations (1.1):

$$h'_t + (hu' + h'\hat{u})_x + (hv' + h'\hat{v})_y = 0, \tag{2.5a}$$

$$(hu)_t + \left(2\hat{h}\hat{u}u' + \hat{h}(u')^2 + h'u^2\right)_x + (\hat{h}\hat{u}v' + \hat{h}u'v + h'uv)_y + \frac{1}{\varepsilon^2}\left[\frac{(h')^2}{2} + (\hat{h} + Z)h'\right]_x = \frac{1}{\varepsilon}(hv - \hat{h}\hat{v}) + \frac{1}{\varepsilon^2}h'_x Z, \tag{2.5b}$$

$$(hv)_t + (\hat{h}\hat{u}v' + \hat{h}u'v + h'uv)_x + \left(2\hat{h}\hat{v}v' + \hat{h}(v')^2 + h'v^2\right)_y + \frac{1}{\varepsilon^2}\left[\frac{(h')^2}{2} + (\hat{h} + Z)h'\right]_y = -\frac{1}{\varepsilon}(hu - \hat{h}\hat{u}) + \frac{1}{\varepsilon^2}h'_y Z. \tag{2.5c}$$

This form of the RSW system will be used to develop a new WB-AP scheme.

2.1 Asymptotic Analysis

We consider the low Froude number regime for the system (2.5) and study its asymptotic limit as $\varepsilon \to 0$.

For the sake of the simplicity, instead of considering the general steady states (2.3), we assume that $\hat{\boldsymbol{w}} := (\hat{h}, \hat{u}, \hat{v})^\top$ is a geostrophic equilibrium satisfying

$$\hat{u}_x + \hat{v}_y = 0, \tag{2.6a}$$

$$\frac{1}{\varepsilon^2}(\hat{h} + Z)_x = \frac{1}{\varepsilon}\hat{v}, \tag{2.6b}$$

$$\frac{1}{\varepsilon^2}(\hat{h} + Z)_y = -\frac{1}{\varepsilon}\hat{u}, \tag{2.6c}$$

which, together with (2.3), implies that

$$\begin{cases} \hat{u}\hat{h}_x + \hat{v}\hat{h}_y = 0, \\ \hat{u}\hat{u}_x + \hat{v}\hat{u}_y = 0, \\ \hat{u}\hat{v}_x + \hat{v}\hat{v}_y = 0. \end{cases} \tag{2.7}$$

In order to investigate the asymptotic limit of the system (2.5), we consider the following asymptotic expansions of both $\boldsymbol{w} := (h, u, v)^\top$ and the geostrophic equilibrium $\hat{\boldsymbol{w}}$:

$$\boldsymbol{w} = \boldsymbol{w}^{(0)} + \varepsilon \boldsymbol{w}^{(1)} + \varepsilon^2 \boldsymbol{w}^{(2)} + \cdots, \tag{2.8}$$

$$\hat{\boldsymbol{w}} = \hat{\boldsymbol{w}}^{(0)} + \varepsilon \hat{\boldsymbol{w}}^{(1)} + \varepsilon^2 \hat{\boldsymbol{w}}^{(2)} + \cdots. \tag{2.9}$$

We first substitute (2.9) into (2.6) and (2.7), and then collect the ε-like powers to obtain

$$\begin{aligned} \mathcal{O}(\varepsilon^{-2}):\ & (\hat{h}^{(0)} + Z)_x = 0, \\ & (\hat{h}^{(0)} + Z)_y = 0, \\ \mathcal{O}(\varepsilon^{-1}):\ & \hat{h}^{(1)}_x = \hat{v}^{(0)}, \\ & \hat{h}^{(1)}_y = -\hat{u}^{(0)}, \\ \mathcal{O}(1):\ & \hat{u}^{(0)}_x + \hat{v}^{(0)}_y = 0, \\ & \hat{u}^{(0)}\hat{h}^{(0)}_x + \hat{v}^{(0)}\hat{h}^{(0)}_y = 0, \\ & \hat{u}^{(0)}\hat{u}^{(0)}_x + \hat{v}^{(0)}\hat{u}^{(0)}_y = 0, \\ & \hat{u}^{(0)}\hat{v}^{(0)}_x + \hat{v}^{(0)}\hat{v}^{(0)}_y = 0, \\ \mathcal{O}(\varepsilon):\ & \hat{u}^{(1)}_x + \hat{v}^{(1)}_y = 0, \\ & \hat{u}^{(0)}\hat{h}^{(1)}_x + \hat{v}^{(0)}\hat{h}^{(1)}_y + \hat{u}^{(1)}\hat{h}^{(0)}_x + \hat{v}^{(1)}\hat{h}^{(0)}_y = 0. \end{aligned} \tag{2.10}$$

Next, we take into account the scaling given by equations (2.6b) and (2.6c) and consider the perturbations to be of the following sizes: $h' = \mathcal{O}(\varepsilon^2)$, $u' = \mathcal{O}(\varepsilon)$ and $v' = \mathcal{O}(\varepsilon)$, so that the asymptotic expansions of $\boldsymbol{w'} := (h', u', v')^\top$ are

$$h' = \varepsilon^2 h'^{(2)} + \cdots, \quad u' = \varepsilon u'^{(1)} + \varepsilon^2 u'^{(2)} + \cdots, \quad v' = \varepsilon v'^{(1)} + \varepsilon^2 v'^{(2)} + \cdots. \tag{2.11}$$

Note that since $\boldsymbol{w} = \hat{\boldsymbol{w}} + \boldsymbol{w'}$, equation (2.11) implies

$$\hat{h}^{(0)} = h^{(0)}, \quad \hat{h}^{(1)} = h^{(1)}, \quad \hat{u}^{(0)} = u^{(0)}, \quad \hat{v}^{(0)} = v^{(0)}. \tag{2.12}$$

Substituting (2.8), (2.9) and (2.11) into the reformulated RSW system (2.5), using (2.10) and (2.12), and once again collecting the ε-like powers, we derive

$$\mathcal{O}(1):\ h'^{(2)}_x = v'^{(1)}, \tag{2.13a}$$

$$h'^{(2)}_y = -u'^{(1)}, \tag{2.13b}$$

$$\mathcal{O}(\varepsilon):\ (\hat{h}^{(0)}u'^{(1)})_t + 2\big(\hat{h}^{(0)}\hat{u}^{(0)}u'^{(1)}\big)_x + \big(\hat{h}^{(0)}\hat{u}^{(0)}v'^{(1)} + \hat{h}^{(0)}u'^{(1)}\hat{v}^{(0)}\big)_y = \hat{h}^{(0)}v'^{(2)}, \tag{2.13c}$$

$$(\hat{h}^{(0)}v'^{(1)})_t + \big(\hat{h}^{(0)}\hat{u}^{(0)}v'^{(1)} + \hat{h}^{(0)}u'^{(1)}\hat{v}^{(0)}\big)_x + 2\big(\hat{h}^{(0)}\hat{v}^{(0)}v'^{(1)}\big)_y = -\hat{h}^{(0)}u'^{(2)}, \tag{2.13d}$$

$$\mathcal{O}(\varepsilon^2):\ h'^{(2)}_t + \big(h'^{(2)}\hat{u}^{(0)} + \hat{h}^{(0)}u'^{(2)} + \hat{h}^{(1)}u'^{(1)}\big)_x + \big(h'^{(2)}\hat{v}^{(0)} + \hat{h}^{(0)}v'^{(2)} + \hat{h}^{(1)}v'^{(1)}\big)_y = 0. \tag{2.13e}$$

Finally, we differentiate equations (2.13c) and (2.13d) with respect to y and x, respectively, and substitute them into (2.13e) to obtain

$$\begin{aligned} h_t'^{(2)} - (\hat{h}^{(0)}v'^{(1)})_{xt} + (\hat{h}^{(0)}u'^{(1)})_{yt} &= 2\big(\hat{h}^{(0)}\hat{v}^{(0)}v'^{(1)} - \hat{h}^{(0)}\hat{u}^{(0)}u'^{(1)}\big)_{xy} \\ &+ \big(\hat{h}^{(0)}\hat{u}^{(0)}v'^{(1)} + \hat{h}^{(0)}\hat{v}^{(0)}u'^{(1)}\big)_{xx} - \big(\hat{h}^{(0)}\hat{u}^{(0)}v'^{(1)} + \hat{h}^{(0)}\hat{v}^{(0)}u'^{(1)}\big)_{yy}. \end{aligned} \tag{2.14}$$

In summary, using (2.13a)–(2.13d) and (2.14) we derive the following equations:

$$\begin{aligned} &u'^{(1)} = -h_y'^{(2)}, \\ &v'^{(1)} = h_x'^{(2)}, \\ &(\hat{h}^{(0)}u'^{(1)})_t + 2\big(\hat{h}^{(0)}\hat{u}^{(0)}u'^{(1)}\big)_x + \big(\hat{h}^{(0)}\hat{u}^{(0)}v'^{(1)} + \hat{h}^{(0)}u'^{(1)}\hat{v}^{(0)}\big)_y = \hat{h}^{(0)}v'^{(2)}, \\ &(\hat{h}^{(0)}v'^{(1)})_t + \big(\hat{h}^{(0)}\hat{u}^{(0)}v'^{(1)} + \hat{h}^{(0)}u'^{(1)}\hat{v}^{(0)}\big)_x + 2\big(\hat{h}^{(0)}\hat{v}^{(0)}v'^{(1)}\big)_y = -\hat{h}^{(0)}u'^{(2)}, \\ &h_t'^{(2)} - (\hat{h}^{(0)}v'^{(1)})_{xt} + (\hat{h}^{(0)}u'^{(1)})_{yt} = 2\big(\hat{h}^{(0)}\hat{v}^{(0)}v'^{(1)} - \hat{h}^{(0)}\hat{u}^{(0)}u'^{(1)}\big)_{xy} \\ &\quad + \big(\hat{h}^{(0)}\hat{u}^{(0)}v'^{(1)} + \hat{h}^{(0)}\hat{v}^{(0)}u'^{(1)}\big)_{xx} - \big(\hat{h}^{(0)}\hat{u}^{(0)}v'^{(1)} + \hat{h}^{(0)}\hat{v}^{(0)}u'^{(1)}\big)_{yy}. \end{aligned} \tag{2.15}$$

3 A Well-Balanced Asymptotic Preserving Scheme

In this section we develop an AP scheme for the RSW system (2.5) and perform an asymptotic analysis to show that the new scheme provides a consistent and stable discretization of the limiting system as the Froude number $\varepsilon \to 0$. We will also show that the proposed AP scheme is WB in the sense that it is capable of preserving the steady states (2.3) at the discrete level.

3.1 Hyperbolic Flux Splitting

In order to construct an AP scheme for the system (2.5), we split the fluxes into two parts corresponding to the slow and fast dynamics:

$$h_t' + \alpha\big[(hu' + h'\hat{u})_x + (hv' + h'\hat{v})_y\big] + (1-\alpha)\big[(hu)_x + (hv)_y\big] = 0, \tag{3.1a}$$

$$\begin{aligned} &(hu)_t + \left(2\hat{h}\hat{u}u' + \hat{h}(u')^2 + h'u^2 + \frac{\frac{(h')^2}{2} + \big(\hat{h} + Z - a(t)\big)h'}{\varepsilon^2}\right)_x + (\hat{h}\hat{u}v' + \hat{h}u'v + h'uv)_y + \frac{a(t)}{\varepsilon^2}h_x' \\ &\quad = \frac{1}{\varepsilon}(hv - \hat{h}\hat{v}) + \frac{1}{\varepsilon^2}h_x'Z, \end{aligned} \tag{3.1b}$$

$$\begin{aligned} &(hv)_t + (\hat{h}\hat{u}v' + \hat{h}u'v + h'uv)_x + \left(2\hat{h}\hat{v}v' + \hat{h}(v')^2 + h'v^2 + \frac{\frac{(h')^2}{2} + \big(\hat{h} + Z - a(t)\big)h'}{\varepsilon^2}\right)_y + \frac{a(t)}{\varepsilon^2}h_y' \\ &\quad = -\frac{1}{\varepsilon}(hu - \hat{h}\hat{u}) + \frac{1}{\varepsilon^2}h_y'Z. \end{aligned} \tag{3.1c}$$

We note that equation (3.1a) is indeed equivalent to equation (2.5a), as the steady-state solution $\hat{\boldsymbol{w}}$ satisfies the relationship (2.3a). The system (3.1) can be rewritten in the following vector form:

$$\boldsymbol{U}_t + \widetilde{\boldsymbol{F}}(\boldsymbol{U})_x + \widetilde{\boldsymbol{G}}(\boldsymbol{U})_y + \breve{\boldsymbol{F}}(\boldsymbol{U})_x + \breve{\boldsymbol{G}}(\boldsymbol{U})_y = \boldsymbol{S}(\boldsymbol{U}),$$

where $\boldsymbol{U} := (h', hu, hv)^\top$ are the conservative variables. The nonstiff fluxes $\widetilde{\boldsymbol{F}}$ and $\widetilde{\boldsymbol{G}}$ governing the slow dynamics and

$$\begin{aligned}
\widetilde{\boldsymbol{F}}(\boldsymbol{U}) &:= \begin{pmatrix} \alpha(hu' + h'\hat{u}) \\ 2\hat{h}\hat{u}u' + \hat{h}(u')^2 + h'u^2 + \dfrac{1}{\varepsilon^2}\left[\dfrac{(h')^2}{2} + \big(\hat{h} + Z - a(t)\big)h'\right] \\ \hat{h}\hat{u}v' + \hat{h}u'v + h'uv \end{pmatrix}, \\
\widetilde{\boldsymbol{G}}(\boldsymbol{U}) &:= \begin{pmatrix} \alpha(hv' + h'\hat{v}) \\ \hat{h}\hat{u}v' + \hat{h}u'v + h'uv \\ 2\hat{h}\hat{v}v' + \hat{h}(v')^2 + h'v^2 + \dfrac{1}{\varepsilon^2}\left[\dfrac{(h')^2}{2} + \big(\hat{h} + Z - a(t)\big)h'\right] \end{pmatrix},
\end{aligned} \tag{3.2}$$

while the stiff fluxes $\breve{\boldsymbol{F}}$ and $\breve{\boldsymbol{G}}$ describing the fast dynamics and the source term $\boldsymbol{S}$ are

$$\breve{\boldsymbol{F}}(\boldsymbol{U}) := \begin{pmatrix} (1-\alpha)hu \\ \dfrac{a(t)}{\varepsilon^2}h' \\ 0 \end{pmatrix}, \quad \breve{\boldsymbol{G}}(\boldsymbol{U}) := \begin{pmatrix} (1-\alpha)hv \\ 0 \\ \dfrac{a(t)}{\varepsilon^2}h' \end{pmatrix}, \quad \boldsymbol{S}(\boldsymbol{U}) := \begin{pmatrix} 0 \\ \dfrac{1}{\varepsilon}(hv - \hat{h}\hat{v}) + \dfrac{1}{\varepsilon^2}h'_x Z \\ -\dfrac{1}{\varepsilon}(hu - \hat{h}\hat{u}) + \dfrac{1}{\varepsilon^2}h'_y Z \end{pmatrix}.$$

Notice that the eigenvalues of the Jacobians $\partial\widetilde{\boldsymbol{F}}/\partial\boldsymbol{U}$ and $\partial\widetilde{\boldsymbol{G}}/\partial\boldsymbol{U}$ are

$$\left\{u, u \pm \sqrt{(1-\alpha)u^2 + \alpha\frac{h' + \hat{h} + Z - a(t)}{\varepsilon^2}}\right\} \tag{3.3}$$

and

$$\left\{v, v \pm \sqrt{(1-\alpha)v^2 + \alpha\frac{h' + \hat{h} + Z - a(t)}{\varepsilon^2}}\right\}, \tag{3.4}$$

respectively. In order to guarantee the hyperbolicity and nonstiffness of the subsystem $\boldsymbol{U}_t + \widetilde{\boldsymbol{F}}(\boldsymbol{U})_x + \widetilde{\boldsymbol{G}}(\boldsymbol{U})_y = \boldsymbol{0}$, the flux splitting parameters α and $a(t)$ should be selected in an appropriate way. We choose

$$\alpha = \min\left(\varepsilon^s, \frac{1}{2}\right) \quad \text{and} \quad a(t) = \min_{(x,y)\in\Omega}\Big(h'(x,y,t) + \hat{h}(x,y) + Z(x,y)\Big), \tag{3.5}$$

where $s \geqslant 1$. As discussed in [32], although one can take any value of $s \geqslant 1$, we set $s = 2$ to guarantee that the stability time-step restriction is independent of ε; see (3.3), (3.4) and (3.5).

3.2 First-Order Implicit-Explicit (IMEX) Time Discretization

In order to derive an efficient discretization of the multiscale RSW equations (3.1) we follow the implicit-explicit (IMEX) approach and approximate the nonstiff flux terms, $\widetilde{\boldsymbol{F}}(\boldsymbol{U})_x$ and $\widetilde{\boldsymbol{G}}(\boldsymbol{U})_y$, explicitly and stiff flux and source terms, $\breve{\boldsymbol{F}}(\boldsymbol{U})_x$, $\breve{\boldsymbol{G}}(\boldsymbol{U})_y$ and $\boldsymbol{S}(\boldsymbol{U})$, implicitly.

We first apply the simplest first-order IMEX method (forward-backward Euler method from [1]) to the system (3.1) and obtain

$$\begin{aligned}
&\frac{(h')^{n+1}-(h')^n}{\Delta t}+\alpha\left[(hu'+h'\hat{u})^n_x+(hv'+h'\hat{v})^n_y\right]+(1-\alpha)\left[(hu)^{n+1}_x+(hv)^{n+1}_y\right]=0,\\
&\frac{(hu)^{n+1}-(hu)^n}{\Delta t}+\left(2\hat{h}\hat{u}u'+\hat{h}(u')^2+h'u^2+\frac{\frac{(h')^2}{2}+\big(\hat{h}+Z-a(t)\big)h'}{\varepsilon^2}\right)^n_x\\
&\qquad+(\hat{h}\hat{u}v'+\hat{h}u'v+h'uv)^n_y+\frac{a(t)}{\varepsilon^2}(h')^{n+1}_x=\frac{1}{\varepsilon}\left[(hv)^{n+1}-\hat{h}\hat{v}\right]+\frac{1}{\varepsilon^2}(h')^{n+1}_xZ,\\
&\frac{(hv)^{n+1}-(hv)^n}{\Delta t}+\left(2\hat{h}\hat{v}v'+\hat{h}(v')^2+h'v^2+\frac{\frac{(h')^2}{2}+\big(\hat{h}+Z-a(t)\big)h'}{\varepsilon^2}\right)^n_y\\
&\qquad+(\hat{h}\hat{u}v'+\hat{h}u'v+h'uv)^n_x+\frac{a(t)}{\varepsilon^2}(h')^{n+1}_y=-\frac{1}{\varepsilon}\left[(hu)^{n+1}-\hat{h}\hat{u}\right]+\frac{1}{\varepsilon^2}(h')^{n+1}_yZ.
\end{aligned}\tag{3.6}$$

Introducing the notation $\boldsymbol{R}^n:=(R^{h',n},R^{hu,n},R^{hv,n})^\top$ we rewrite the system (3.6) as

$$\begin{aligned}
&\frac{(h')^{n+1}-(h')^n}{\Delta t}-R^{h',n}+(1-\alpha)\left[(hu)^{n+1}_x+(hv)^{n+1}_y\right]=0,\\
&\frac{(hu)^{n+1}-(hu)^n}{\Delta t}-R^{hu,n}+\frac{a(t)}{\varepsilon^2}(h')^{n+1}_x=\frac{1}{\varepsilon}\left[(hv)^{n+1}-\hat{h}\hat{v}\right]+\frac{1}{\varepsilon^2}(h')^{n+1}_xZ,\\
&\frac{(hv)^{n+1}-(hv)^n}{\Delta t}-R^{hv,n}+\frac{a(t)}{\varepsilon^2}(h')^{n+1}_y=-\frac{1}{\varepsilon}\left[(hu)^{n+1}-\hat{h}\hat{u}\right]+\frac{1}{\varepsilon^2}(h')^{n+1}_yZ,
\end{aligned}\tag{3.7}$$

where

$$\begin{aligned}
&R^{h',n}:=-\alpha\left[(hu'+h'\hat{u})^n_x+(hv'+h'\hat{v})^n_y\right],\\
&R^{hu,n}:=-\left(2\hat{h}\hat{u}u'+\hat{h}(u')^2+h'u^2+\frac{\frac{(h')^2}{2}+\big(\hat{h}+Z-a(t)\big)h'}{\varepsilon^2}\right)^n_x-(\hat{h}\hat{u}v'+\hat{h}u'v+h'uv)^n_y,\\
&R^{hv,n}:=-(\hat{h}\hat{u}v'+\hat{h}u'v+h'uv)^n_x-\left(2\hat{h}\hat{v}v'+\hat{h}(v')^2+h'v^2+\frac{\frac{(h')^2}{2}+\big(\hat{h}+Z-a(t)\big)h'}{\varepsilon^2}\right)^n_y.
\end{aligned}$$

The remaining part of Section 3 is organized as follows. In Section 3.3 we describe the CU spatial discretization of the nonstiff flux terms. In Section 3.4 we present and analyze the fully-discrete second-order IMEX WB-AP CU scheme for the studied RSW equations.

3.3 Central-Upwind (CU) Discretization of the Nonstiff Flux Terms

We use the second-order finite volume CU scheme to discretize the nonstiff fluxes (3.2). To this end we introduce a Cartesian mesh with the uniform (for the sake of simplicity) cells $C_{j,k}:=[x_{j-\frac12},x_{j+\frac12}]\times[y_{k-\frac12},y_{k+\frac12}]$ of size $\big|C_{j,k}\big|=\Delta x\Delta y$ centered at the grid points (x_j,y_k) with $x_j:=(x_{j+\frac12}+x_{j-\frac12})/2$ and $y_k:=(y_{k+\frac12}+y_{k-\frac12})/2$. First, we use the following notation for the point values of $\hat{h}$ at the cell centers and cell interfaces:

$$\hat{h}_{j,k}:=\hat{h}(x_j,y_k),\quad \hat{h}_{j+\frac12,k}:=\hat{h}(x_{j+\frac12},y_k),\quad \hat{h}_{j,k+\frac12}:=\hat{h}(x_j,y_{k+\frac12}),$$

and analogous notations for $\hat{u}$ and $\hat{v}$. For the point values of the bottom topography at the cell corners we set

$$Z_{j+\frac{1}{2},k+\frac{1}{2}} := Z(x_{j+\frac{1}{2}}, y_{k+\frac{1}{2}}), \tag{3.8}$$

and the point values of Z at the cell centers and cell interfaces are approximated using a continuous bilinear interpolant; see [23, 26]:

$$\begin{aligned}
&Z_{j,k} := \frac{1}{4}\left(Z_{j+\frac{1}{2},k+\frac{1}{2}} + Z_{j+\frac{1}{2},k-\frac{1}{2}} + Z_{j-\frac{1}{2},k+\frac{1}{2}} + Z_{j-\frac{1}{2},k-\frac{1}{2}}\right),\\
&Z_{j+\frac{1}{2},k} := \frac{1}{2}\left(Z_{j+\frac{1}{2},k+\frac{1}{2}} + Z_{j+\frac{1}{2},k-\frac{1}{2}}\right), \quad Z_{j,k+\frac{1}{2}} := \frac{1}{2}\left(Z_{j+\frac{1}{2},k+\frac{1}{2}} + Z_{j-\frac{1}{2},k+\frac{1}{2}}\right).
\end{aligned}$$

Remark 3.1 *We note that formula (3.8) is only valid when the bottom topography function is continuous. In the case of discontinuous Z, we refer the reader to [23, 26].*

We assume that at time level $t = t^n$ the numerical solution is realized in terms of its cell averages denoted by

$$\overline{\boldsymbol{U}}^n_{j,k} :\approx \frac{1}{\Delta x \Delta y}\iint\limits_{C_{j,k}} \boldsymbol{U}(x, y, t^n)\,\mathrm{d}x\,\mathrm{d}y.$$

In each cell we approximate the flux contribution $\boldsymbol{R} := -\widetilde{\boldsymbol{F}}(\boldsymbol{U})_x - \widetilde{\boldsymbol{G}}(\boldsymbol{U})_y$ by

$$\boldsymbol{\mathcal{R}}^n_{j,k} := -\frac{\widetilde{\boldsymbol{\mathcal{F}}}^n_{j+\frac{1}{2},k} - \widetilde{\boldsymbol{\mathcal{F}}}^n_{j-\frac{1}{2},k}}{\Delta x} - \frac{\widetilde{\boldsymbol{\mathcal{G}}}^n_{j,k+\frac{1}{2}} - \widetilde{\boldsymbol{\mathcal{G}}}^n_{j,k-\frac{1}{2}}}{\Delta y}, \tag{3.9}$$

where $\widetilde{\boldsymbol{\mathcal{F}}}^n_{j+\frac{1}{2},k}$ and $\widetilde{\boldsymbol{\mathcal{G}}}^n_{j,k+\frac{1}{2}}$ are the CU numerical fluxes in the x- and y-directions, respectively. We use the CU numerical fluxes from [29] (see also [15] for a one-dimensional first-order version):

$$\begin{aligned}
\widetilde{\boldsymbol{\mathcal{F}}}^n_{j+\frac{1}{2},k} &= \frac{a^+_{j+\frac{1}{2},k}\widetilde{\boldsymbol{F}}(\boldsymbol{U}^{\mathrm{E}}_{j,k}) - a^-_{j+\frac{1}{2},k}\widetilde{\boldsymbol{F}}(\boldsymbol{U}^{\mathrm{W}}_{j+1,k})}{a^+_{j+\frac{1}{2},k} - a^-_{j+\frac{1}{2},k}} + \frac{a^+_{j+\frac{1}{2},k}a^-_{j+\frac{1}{2},k}}{a^+_{j+\frac{1}{2},k} - a^-_{j+\frac{1}{2},k}}\left[\boldsymbol{U}^{\mathrm{W}}_{j+1,k} - \boldsymbol{U}^{\mathrm{E}}_{j,k}\right],\\
\widetilde{\boldsymbol{\mathcal{G}}}^n_{j,k+\frac{1}{2}} &= \frac{b^+_{j,k+\frac{1}{2}}\widetilde{\boldsymbol{G}}(\boldsymbol{U}^{\mathrm{N}}_{j,k}) - b^-_{j,k+\frac{1}{2}}\widetilde{\boldsymbol{G}}(\boldsymbol{U}^{\mathrm{S}}_{j,k+1})}{b^+_{j,k+\frac{1}{2}} - b^-_{j,k+\frac{1}{2}}} + \frac{b^+_{j,k+\frac{1}{2}}b^-_{j,k+\frac{1}{2}}}{b^+_{j,k+\frac{1}{2}} - b^-_{j,k+\frac{1}{2}}}\left[\boldsymbol{U}^{\mathrm{S}}_{j,k+1} - \boldsymbol{U}^{\mathrm{N}}_{j,k}\right].
\end{aligned} \tag{3.10}$$

Note that all of the quantities on the right-hand side (RHS) are computed at time level t^n, but we omit this information for the sake of brevity. We will do the same in the rest of the paper: all of the indexed quantities in which the time level is not explicitly specified, will be assumed to be taken at $t = t^n$.

In (3.10) $\boldsymbol{U}^{\mathrm{E}}_{j,k}$, $\boldsymbol{U}^{\mathrm{W}}_{j,k}$, $\boldsymbol{U}^{\mathrm{N}}_{j,k}$ and $\boldsymbol{U}^{\mathrm{S}}_{j,k}$ stand for the point values of $\boldsymbol{U}$, which are supposed to be reconstructed from the given cell averages $\left\{\overline{(h')}_{j,k}, \overline{(hu)}_{j,k}, \overline{(hv)}_{j,k}\right\}$. In order to ensure the WB property of the resulting scheme, we perform the reconstruction in the equilibrium variables $\boldsymbol{w'}$, which remain constant (in fact, zero) at the steady states, which guarantees the WB property of the resulting scheme as shown in Section 3.4.1. To this end we first compute the point values of u' and v' at the cell centers:

$$u'_{j,k} = \frac{\overline{(hu)}_{j,k}}{\overline{h'}_{j,k} + \hat{h}_{j,k}} - \hat{u}_{j,k}, \qquad v'_{j,k} = \frac{\overline{(hv)}_{j,k}}{\overline{h'}_{j,k} + \hat{h}_{j,k}} - \hat{v}_{j,k},$$

and then construct a global piecewise linear reconstruction

$$\widetilde{\boldsymbol{w}'}(x,y) := \overline{\boldsymbol{w}'}_{j,k} + (\boldsymbol{w}'_x)_{j,k}(x-x_j) + (\boldsymbol{w}'_y)_{j,k}(y-y_k), \quad (x,y) \in C_{j,k}, \tag{3.11}$$

where $(\boldsymbol{w}'_x)_{j,k}$ and $(\boldsymbol{w}'_y)_{j,k}$ are at least first-order approximations of the derivatives $\boldsymbol{w}'_x(x_j,y_k,t^n)$ and $\boldsymbol{w}'_y(x_j,y_k,t^n)$, respectively. In order to ensure a non-oscillatory nature of the reconstruction (3.11), the slopes are supposed to be computed using nonlinear limiter. In the numerical experiments reported in Section 4 we have used the generalized minmod limiter [31, 35, 40, 42]:

$$\begin{aligned}
(\boldsymbol{w}'_x)_{j,k} &= \text{minmod}\left(\theta\,\frac{\boldsymbol{w}'_{j,k}-\boldsymbol{w}'_{j-1,k}}{\Delta x}, \frac{\boldsymbol{w}'_{j+1,k}-\boldsymbol{w}'_{j-1,k}}{2\Delta x}, \theta\,\frac{\boldsymbol{w}'_{j+1,k}-\boldsymbol{w}'_{j,k}}{\Delta x}\right),\\
(\boldsymbol{w}'_y)_{j,k} &= \text{minmod}\left(\theta\,\frac{\boldsymbol{w}'_{j,k}-\boldsymbol{w}'_{j,k-1}}{\Delta y}, \frac{\boldsymbol{w}'_{j,k+1}-\boldsymbol{w}'_{j,k-1}}{2\Delta y}, \theta\,\frac{\boldsymbol{w}'_{j,k+1}-\boldsymbol{w}'_{j,k}}{\Delta y}\right),
\end{aligned} \tag{3.12}$$

where the minmod function, defined by

$$\text{minmod}(\varphi_1,\varphi_2,\ldots) := \begin{cases} \min\limits_k\{\varphi_k\}, & \text{if } \varphi_k > 0 \ \ \forall k,\\ \max\limits_k\{\varphi_k\}, & \text{if } \varphi_k < 0 \ \ \forall k,\\ 0, & \text{otherwise,}\end{cases}$$

is applied in a componentwise manner. In (3.12) the parameter $\theta \in [1,2]$ helps to control the amount of numerical diffusion: larger values of θ correspond to less diffusive, but more oscillatory reconstructions. In the numerical examples reported in Section 4, we have taken $\theta = 2$.

Applying the reconstruction (3.11) we obtain the following point values of $\boldsymbol{w}'$:

$$\begin{aligned}
(\boldsymbol{w}')^{\rm E}_{j,k} &= \widetilde{\boldsymbol{w}'}(x_{j+\frac12},y_k) = \overline{\boldsymbol{w}'}_{j,k} + \frac{\Delta x}{2}(\boldsymbol{w}'_x)_{j,k}, \quad (\boldsymbol{w}')^{\rm W}_{j,k} = \widetilde{\boldsymbol{w}'}(x_{j-\frac12},y_k) = \overline{\boldsymbol{w}'}_{j,k} - \frac{\Delta x}{2}(\boldsymbol{w}'_x)_{j,k},\\
(\boldsymbol{w}')^{\rm N}_{j,k} &= \widetilde{\boldsymbol{w}'}(x_j,y_{k+\frac12}) = \overline{\boldsymbol{w}'}_{j,k} + \frac{\Delta y}{2}(\boldsymbol{w}'_y)_{j,k}, \quad (\boldsymbol{w}')^{\rm S}_{j,k} = \widetilde{\boldsymbol{w}'}(x_j,y_{k-\frac12}) = \overline{\boldsymbol{w}'}_{j,k} - \frac{\Delta y}{2}(\boldsymbol{w}'_y)_{j,k},
\end{aligned}$$

which, together with the corresponding point values of the given steady state, are used to evaluate

$$\begin{aligned}
(hu)^{\rm E}_{j,k} &= \big(\hat h_{j+\frac12,k} + (h')^{\rm E}_{j,k}\big)\big(\hat u_{j+\frac12,k} + (u')^{\rm E}_{j,k}\big), \quad (hv)^{\rm E}_{j,k} = \big(\hat h_{j+\frac12,k} + (h')^{\rm E}_{j,k}\big)\big(\hat v_{j+\frac12,k} + (v')^{\rm E}_{j,k}\big),\\
(hu)^{\rm W}_{j,k} &= \big(\hat h_{j-\frac12,k} + (h')^{\rm W}_{j,k}\big)\big(\hat u_{j-\frac12,k} + (u')^{\rm W}_{j,k}\big), \quad (hv)^{\rm W}_{j,k} = \big(\hat h_{j-\frac12,k} + (h')^{\rm W}_{j,k}\big)\big(\hat v_{j-\frac12,k} + (v')^{\rm W}_{j,k}\big),\\
(hu)^{\rm N}_{j,k} &= \big(\hat h_{j,k+\frac12} + (h')^{\rm N}_{j,k}\big)\big(\hat u_{j,k+\frac12} + (u')^{\rm N}_{j,k}\big), \quad (hv)^{\rm N}_{j,k} = \big(\hat h_{j,k+\frac12} + (h')^{\rm N}_{j,k}\big)\big(\hat v_{j,k+\frac12} + (v')^{\rm N}_{j,k}\big),\\
(hu)^{\rm S}_{j,k} &= \big(\hat h_{j,k-\frac12} + (h')^{\rm S}_{j,k}\big)\big(\hat u_{j,k-\frac12} + (u')^{\rm S}_{j,k}\big), \quad (hv)^{\rm S}_{j,k} = \big(\hat h_{j,k-\frac12} + (h')^{\rm S}_{j,k}\big)\big(\hat v_{j,k-\frac12} + (v')^{\rm S}_{j,k}\big).
\end{aligned}$$

Finally, $a^{\pm}_{j+\frac12,k}$ and $b^{\pm}_{j,k+\frac12}$, required in the computation of the numerical fluxes (3.10), are the one-sided local propagation speeds, which we estimate using the smallest and largest eigenvalues

of the Jacobians $\partial\widetilde{\boldsymbol{F}}/\partial\boldsymbol{U}$ and $\partial\widetilde{\boldsymbol{G}}/\partial\boldsymbol{U}$, (3.3) and (3.4), as follows:

$$
\begin{aligned}
a^+_{j+\frac12,k} &= \max\left\{u^{\rm E}_{j,k}+\sqrt{(1-\alpha)\big(u^{\rm E}_{j,k}\big)^2+\alpha\,\frac{(h')^{\rm E}_{j,k}+\hat h_{j+\frac12,k}+Z_{j+\frac12,k}-a^n}{\varepsilon^2}},\right.\\
&\qquad\left. u^{\rm W}_{j+1,k}+\sqrt{(1-\alpha)\big(u^{\rm W}_{j+1,k}\big)^2+\alpha\,\frac{(h')^{\rm W}_{j+1,k}+\hat h_{j+\frac12,k}+Z_{j+\frac12,k}-a^n}{\varepsilon^2}},\,0\right\},\\
a^-_{j+\frac12,k} &= \min\left\{u^{\rm E}_{j,k}-\sqrt{(1-\alpha)\big(u^{\rm E}_{j,k}\big)^2+\alpha\,\frac{(h')^{\rm E}_{j,k}+\hat h_{j+\frac12,k}+Z_{j+\frac12,k}-a^n}{\varepsilon^2}},\right.\\
&\qquad\left. u^{\rm W}_{j+1,k}-\sqrt{(1-\alpha)\big(u^{\rm W}_{j+1,k}\big)^2+\alpha\,\frac{(h')^{\rm W}_{j+1,k}+\hat h_{j+\frac12,k}+Z_{j+\frac12,k}-a^n}{\varepsilon^2}},\,0\right\},\\
b^+_{j,k+\frac12} &= \max\left\{v^{\rm N}_{j,k}+\sqrt{(1-\alpha)\big(v^{\rm N}_{j,k}\big)^2+\alpha\,\frac{(h')^{\rm N}_{j,k}+\hat h_{j,k+\frac12}+Z_{j,k+\frac12}-a^n}{\varepsilon^2}},\right.\\
&\qquad\left. v^{\rm S}_{j,k+1}+\sqrt{(1-\alpha)\big(v^{\rm S}_{j,k+1}\big)^2+\alpha\,\frac{(h')^{\rm S}_{j,k+1}+\hat h_{j,k+\frac12}+Z_{j,k+\frac12}-a^n}{\varepsilon^2}},\,0\right\},\\
b^-_{j,k+\frac12} &= \min\left\{v^{\rm N}_{j,k}-\sqrt{(1-\alpha)\big(v^{\rm N}_{j,k}\big)^2+\alpha\,\frac{(h')^{\rm N}_{j,k}+\hat h_{j,k+\frac12}+Z_{j,k+\frac12}-a^n}{\varepsilon^2}},\right.\\
&\qquad\left. v^{\rm S}_{j,k+1}-\sqrt{(1-\alpha)\big(v^{\rm S}_{j,k+1}\big)^2+\alpha\,\frac{(h')^{\rm S}_{j,k+1}+\hat h_{j,k+\frac12}+Z_{j,k+\frac12}-a^n}{\varepsilon^2}},\,0\right\},
\end{aligned}
\tag{3.13}
$$

where $a^n := a(t^n)$.

3.3.1 Numerical Diffusion of the CU Discretization (3.9)–(3.13)

In this section we analyze the leading order of the numerical diffusion present in the CU discretization (3.9)–(3.13). To this end we first rewrite the CU fluxes (3.10) as

$$
\begin{aligned}
\widetilde{\boldsymbol{\mathcal{F}}}^n_{j+\frac12,k} &= \frac{\widetilde{\boldsymbol{F}}(\boldsymbol{U}^n_{j,k})+\widetilde{\boldsymbol{F}}(\boldsymbol{U}^n_{j+1,k})}{2}+\boldsymbol{\mathcal{D}}^n_{j+\frac12,k},\\
\widetilde{\boldsymbol{\mathcal{G}}}^n_{j,k+\frac12} &= \frac{\widetilde{\boldsymbol{G}}(\boldsymbol{U}^n_{j,k})+\widetilde{\boldsymbol{G}}(\boldsymbol{U}^n_{j,k+1})}{2}+\boldsymbol{\mathcal{D}}^n_{j,k+\frac12},
\end{aligned}
\tag{3.14}
$$

where the corresponding numerical diffusion terms, denoted by $\boldsymbol{\mathcal{D}}^n_{j+\frac12,k}$ and $\boldsymbol{\mathcal{D}}^n_{j,k+\frac12}$, are

$$
\begin{aligned}
\boldsymbol{\mathcal{D}}^n_{j+\frac12,k} &= \frac{a^+_{j+\frac12,k}}{2(a^+_{j+\frac12,k}-a^-_{j+\frac12,k})}\Big[2\widetilde{\boldsymbol{F}}(\boldsymbol{U}^E_{j,k})-\widetilde{\boldsymbol{F}}(\boldsymbol{U}^n_{j,k})-\widetilde{\boldsymbol{F}}(\boldsymbol{U}^n_{j+1,k})\Big]\\
&\quad-\frac{a^-_{j+\frac12,k}}{2(a^+_{j+\frac12,k}-a^-_{j+\frac12,k})}\Big[2\widetilde{\boldsymbol{F}}(\boldsymbol{U}^W_{j+1,k})-\widetilde{\boldsymbol{F}}(\boldsymbol{U}^n_{j,k})-\widetilde{\boldsymbol{F}}(\boldsymbol{U}^n_{j+1,k})\Big]
\end{aligned}
\tag{3.15a}
$$

$$
\begin{aligned}
&+\frac{a^+_{j+\frac12,k}a^-_{j+\frac12,k}}{(a^+_{j+\frac12,k}-a^-_{j+\frac12,k})}\left(\boldsymbol{U}^W_{j+1,k}-\boldsymbol{U}^E_{j,k}\right),\\
\boldsymbol{\mathcal{D}}^n_{j,k+\frac12}&=\frac{b^+_{j,k+\frac12}}{2(b^+_{j,k+\frac12}-b^-_{j,k+\frac12})}\left[2\widetilde{\boldsymbol{G}}(\boldsymbol{U}^N_{j,k})-\widetilde{\boldsymbol{G}}(\boldsymbol{U}^n_{j,k})-\widetilde{\boldsymbol{G}}(\boldsymbol{U}^n_{j,k+1})\right]\\
&-\frac{b^-_{j,k+\frac12}}{2(b^+_{j,k+\frac12}-b^-_{j,k+\frac12})}\left[2\widetilde{\boldsymbol{G}}(\boldsymbol{U}^S_{j,k+1})-\widetilde{\boldsymbol{G}}(\boldsymbol{U}^n_{j,k})-\widetilde{\boldsymbol{G}}(\boldsymbol{U}^n_{j,k+1})\right] \qquad (3.15b)\\
&+\frac{b^+_{j,k+\frac12}b^-_{j,k+\frac12}}{(b^+_{j,k+\frac12}-b^-_{j,k+\frac12})}\left(\boldsymbol{U}^S_{j,k+1}-\boldsymbol{U}^N_{j,k}\right).
\end{aligned}
$$

We proceed by formulating the following asymptotic expansion result.

Proposition 3.2 *In both the x- and y-directions the leading orders of the numerical diffusion are $\mathcal{O}(\varepsilon^2)$, $\mathcal{O}(\varepsilon)$ and $\mathcal{O}(\varepsilon)$ for the first, second and third components, respectively. Furthermore, $\boldsymbol{\mathcal{R}}^n_{j,k}$ defined in (3.9) can be written as*

$$
\boldsymbol{\mathcal{R}}^n_{j,k}=-D_x\widetilde{\boldsymbol{F}}^n_{j,k}-D_y\widetilde{\boldsymbol{G}}^n_{j,k}+\boldsymbol{\mathcal{Q}}^n_{j,k}, \qquad (3.16)
$$

where D_x and D_y are the standard second-order central difference operators and given by

$$
D_x\varphi_{j,k}:=\frac{\varphi_{j+1,k}-\varphi_{j-1,k}}{2\Delta x},\quad D_y\varphi_{j,k}:=\frac{\varphi_{j,k+1}-\varphi_{j,k-1}}{2\Delta y}. \qquad (3.17)
$$

The total numerical diffusion is

$$
\boldsymbol{\mathcal{Q}}^n_{j,k}:=\frac{\boldsymbol{\mathcal{D}}^n_{j+\frac12,k}-\boldsymbol{\mathcal{D}}^n_{j-\frac12,k}}{\Delta x}+\frac{\boldsymbol{\mathcal{D}}^n_{j,k+\frac12}-\boldsymbol{\mathcal{D}}^n_{j,k-\frac12}}{\Delta y},
$$

where each component is expanded with respect to ε as follows:

$$
\begin{aligned}
\mathcal{Q}^{h',n}_{j,k}&=\varepsilon^2\mathcal{Q}^{h',(2),n}+\varepsilon^3\mathcal{Q}^{h',(3),n}+\cdots,\\
\mathcal{Q}^{hu,n}_{j,k}&=\varepsilon\mathcal{Q}^{hu,(1),n}+\varepsilon^2\mathcal{Q}^{hu,(2),n}+\cdots,\\
\mathcal{Q}^{hv,n}_{j,k}&=\varepsilon\mathcal{Q}^{hv,(1),n}+\varepsilon^2\mathcal{Q}^{hv,(2),n}+\cdots.
\end{aligned} \qquad (3.18)
$$

The proof of this proposition follows the lines of the proof in [32, Section 3.4.1] with several obvious changes; see Appendix A.

Remark 3.1 We would like to stress that all of the terms in the expansions (3.18) are proportional to $\Delta^2_{\max}$, where $\Delta_{\max}:=\max(\Delta x,\Delta y)$, since they are introduced by the second-order CU discretization.

3.4 Fully Discrete Well-Balanced Asymptotic Preserving Schemes

In order to derive a fully discrete WB-AP scheme we first solve the second and third equations in (3.7) for $(hu)^{n+1}$ and $(hv)^{n+1}$ to obtain

$$(h')^{n+1} = (h')^n + \Delta t R^{h',n} - \Delta t(1-\alpha)\left[(hu)_x^{n+1} + (hv)_y^{n+1}\right], \tag{3.19a}$$

$$\begin{aligned}(hu)^{n+1} = {}& \hat{h}\hat{u} + \frac{1}{K}\Big[\hat{h}(u')^n + (h'u)^n + \frac{\Delta t}{\varepsilon}\big(\hat{h}(v')^n + (h'v)^n\big) + \Delta t\Big(R^{hu,n} + \frac{\Delta t}{\varepsilon}R^{hv,n}\Big)\\ &+ \frac{(Z-a^n)\Delta t}{\varepsilon^2}\Big((h')_x^{n+1} + \frac{\Delta t}{\varepsilon}(h')_y^{n+1}\Big)\Big],\end{aligned} \tag{3.19b}$$

$$\begin{aligned}(hv)^{n+1} = {}& \hat{h}\hat{v} + \frac{1}{K}\Big[\hat{h}(v')^n + (h'v)^n - \frac{\Delta t}{\varepsilon}\big(\hat{h}(u')^n + (h'u)^n\big) + \Delta t\Big(R^{hv,n} - \frac{\Delta t}{\varepsilon}R^{hu,n}\Big)\\ &+ \frac{(Z-a^n)\Delta t}{\varepsilon^2}\Big((h')_y^{n+1} - \frac{\Delta t}{\varepsilon}(h')_x^{n+1}\Big)\Big],\end{aligned} \tag{3.19c}$$

where $K := 1 + (\Delta t/\varepsilon)^2$. Differentiating equations (3.19b) and (3.19c) with respect to x and y, respectively, and then substituting the obtained results into (3.19a) to end up with the following elliptic equation for $(h')^{n+1}$:

$$\begin{aligned}&(h')^{n+1} + \frac{(Z-a^n)(1-\alpha)}{\widetilde{K}}\big((h')_{xx}^{n+1} + (h')_{yy}^{n+1}\big)\\ &\quad+ \frac{1-\alpha}{\widetilde{K}}\Big[(h')_x^{n+1}Z_x + (h')_y^{n+1}Z_y + \frac{\Delta t}{\varepsilon}\big((h')_y^{n+1}Z_x - (h')_x^{n+1}Z_y\big)\Big]\\ &\quad= (h')^n + \Delta t R^{h',n} - \frac{\Delta t(1-\alpha)}{K}\Big[(\hat{h}u' + h'u)_x^n + (\hat{h}v' + h'v)_y^n + \frac{\Delta t}{\varepsilon}\big((\hat{h}v' + h'v)_x^n\\ &\quad- (\hat{h}u' + h'u)_y^n\big) + \Delta t\left(R_x^{hu,n} + R_y^{hv,n}\right) + \frac{(\Delta t)^2}{\varepsilon}\left(R_x^{hv,n} - R_y^{hu,n}\right)\Big],\end{aligned} \tag{3.20}$$

where $\widetilde{K} := 1 + (\varepsilon/\Delta t)^2$. In order to discretize equation (3.20) we use the second-order CU numerical fluxes given by equations (3.9)–(3.13) to approximate the corresponding nonstiff flux terms $R^{h',n}$, $R^{hu,n}$ and $R^{hv,n}$. Further, the spatial derivatives in (3.20) are approximated using the standard second-order central difference operators D_x and D_y defined in (3.17). This results in

$$\begin{aligned}&\overline{(h')}_{j,k}^{n+1} + \frac{(Z_{j,k}-a^n)(1-\alpha)}{\widetilde{K}}\widetilde{\Delta}\,\overline{(h')}_{j,k}^{n+1}\\ &\quad+ \frac{1-\alpha}{\widetilde{K}}\Big[\Big(D_x - \frac{\Delta t}{\varepsilon}D_y\Big)Z_{j,k}D_x\,\overline{(h')}_{j,k}^{n+1} + \Big(D_y + \frac{\Delta t}{\varepsilon}D_x\Big)Z_{j,k}D_y\,\overline{(h')}_{j,k}^{n+1}\Big]\\ &\quad= \overline{(h')}_{j,k}^{n} + \Delta t\mathcal{R}_{j,k}^{h',n} - \frac{\Delta t(1-\alpha)}{K}\Big[D_x(\hat{h}u' + h'u)_{j,k}^n + D_y(\hat{h}v' + h'v)_{j,k}^n\\ &\quad+ \frac{\Delta t}{\varepsilon}\Big(D_x(\hat{h}v' + h'v)_{j,k}^n - D_y(\hat{h}u' + h'u)_{j,k}^n\Big)\\ &\quad+ \Delta t\left(D_x\mathcal{R}_{j,k}^{hu,n} + D_y\mathcal{R}_{j,k}^{hv,n}\right) + \frac{(\Delta t)^2}{\varepsilon}\left(D_x\mathcal{R}_{j,k}^{hv,n} - D_y\mathcal{R}_{j,k}^{hu,n}\right)\Big],\end{aligned} \tag{3.21}$$

where $\boldsymbol{\mathcal{R}}_{j,k}^n = \big(\mathcal{R}_{j,k}^{h',n}, \mathcal{R}_{j,k}^{hu,n}, \mathcal{R}_{j,k}^{hv,n}\big)^\top$ is defined in (3.9), (3.10) and $\widetilde{\Delta}$ is the discrete five-point Laplacian:

$$\widetilde{\Delta}\varphi_{j,k} := \frac{\varphi_{j+1,k} - 2\varphi_{j,k} + \varphi_{j-1,k}}{(\Delta x)^2} + \frac{\varphi_{j,k+1} - 2\varphi_{j,k} + \varphi_{j,k-1}}{(\Delta y)^2}.$$

Substituting the solution $\overline{(h')}_{j,k}^{n+1}$ of (3.21) into equations (3.19b) and (3.19c) and applying the standard central differences yield

$$\overline{(hu)}_{j,k}^{n+1} = \hat{h}_{j,k}\hat{u}_{j,k} + \frac{1}{K}\Big[\big(\hat{h}u' + h'u\big)_{j,k}^{n} + \frac{\Delta t}{\varepsilon}\big(\hat{h}v' + h'v\big)_{j,k}^{n} + \Delta t\Big(\mathcal{R}_{j,k}^{hu,n} + \frac{\Delta t}{\varepsilon}\mathcal{R}_{j,k}^{hv,n}\Big) + \frac{(Z_{j,k}-a^n)\Delta t}{\varepsilon^2}\Big(D_x\,\overline{(h')}_{j,k}^{n+1} + \frac{\Delta t}{\varepsilon}D_y\,\overline{(h')}_{j,k}^{n+1}\Big)\Big], \tag{3.22}$$

$$\overline{(hv)}_{j,k}^{n+1} = \hat{h}_{j,k}\hat{v}_{j,k} + \frac{1}{K}\Big[\big(\hat{h}v' + h'v\big)_{j,k}^{n} - \frac{\Delta t}{\varepsilon}\big(\hat{h}u' + h'u\big)_{j,k}^{n} + \Delta t\Big(\mathcal{R}_{j,k}^{hv,n} - \frac{\Delta t}{\varepsilon}\mathcal{R}_{j,k}^{hu,n}\Big) + \frac{(Z_{j,k}-a^n)\Delta t}{\varepsilon^2}\Big(D_y\,\overline{(h')}_{j,k}^{n+1} - \frac{\Delta t}{\varepsilon}D_x\,\overline{(h')}_{j,k}^{n+1}\Big)\Big]. \tag{3.23}$$

Notice that the scheme (3.21)–(3.23) is second-order accurate in space, but only first-order accurate in time. In order to increase a temporal accuracy to the second order, we implement a two-stage globally stiffly accurate IMEX Runge-Kutta scheme ARS(2,2,2), which can be described by the following Butcher tableau:

$$\begin{array}{c|ccc||ccc} 0 & 0 & 0 & 0 & 0 & 0 & 0 \\ \gamma & \gamma & 0 & 0 & 0 & \gamma & 0 \\ 1 & 1-\frac{1}{2\gamma} & \frac{1}{2\gamma} & 0 & 0 & 1-\gamma & \gamma \\ \hline & 1-\frac{1}{2\gamma} & \frac{1}{2\gamma} & 0 & 0 & 1-\gamma & \gamma \end{array}$$

where $\gamma = 1-1/\sqrt{2}$; see [1]. Details on the implementation of the ARS(2,2,2) method are provided in Appendix B.

3.4.1 Well-Balanced Property

In this section we prove that the proposed WB-AP CU scheme is indeed WB. To this end we assume that the solution at the time level $t = t^n$ is at the discrete equilibrium, that is,

$$\overline{(h')}_{j,k}^{,n} \equiv 0, \quad (u')_{j,k}^{n} \equiv 0, \quad (v')_{j,k}^{n} \equiv 0, \quad \text{for all } j,k. \tag{3.24}$$

Consequently, from (3.2), (3.9) and (3.10) it follows that

$$\mathcal{R}_{j,k}^{h',n} = 0, \quad \mathcal{R}_{j,k}^{hu,n} = 0, \quad \mathcal{R}_{j,k}^{hv,n} = 0, \quad \text{for all } j,k.$$

Hence, the linear algebraic system (3.21) for $\overline{(h')}_{j,k}$ reduces to

$$\overline{(h')}_{j,k}^{n+1} + \frac{1-\alpha}{\widetilde{K}}\Big[(Z_{j,k}-a^n)\widetilde{\Delta}\,\overline{(h')}_{j,k}^{n+1} + (D_x - \frac{\Delta t}{\varepsilon}D_y)Z_{j,k}D_x\,\overline{(h')}_{j,k}^{n+1} + (D_y + \frac{\Delta t}{\varepsilon}D_x)Z_{j,k}D_y\,\overline{(h')}_{j,k}^{n+1}\Big] = 0,$$

which has a unique solution

$$\overline{(h')}_{j,k}^{n+1} \equiv 0, \quad \text{for all } j,k. \tag{3.25}$$

Finally, substituting (3.24)–(3.25) into (3.22) and (3.23) yields

$$\overline{(hu)}_{j,k}^{n+1} = \hat{h}_{j,k}\hat{u}_{j,k}, \quad \overline{(hv)}_{j,k}^{n+1} = \hat{h}_{j,k}\hat{v}_{j,k}, \quad \text{for all } j,k,$$

which implies that

$$(u')^{n+1}_{j,k} \equiv 0, \quad (v')^{n+1}_{j,k} \equiv 0, \quad \text{for all } j,k.$$

This together with (3.25) completes the proof of the WB property of the proposed scheme.

3.4.2 The Discrete Low Froude Number Limit

In this section we study the discrete low Froude number limit and prove the AP property of the WB-AP CU scheme.

We assume that the geostrophic steady-state $\hat{\boldsymbol{w}}$ admits the same discrete asymptotic expansions as in (2.9):

$$\begin{aligned}
\hat{h}_{J,K} &= \hat{h}^{(0)}_{J,K} + \varepsilon\hat{h}^{(1)}_{J,K} + \varepsilon^2\hat{h}^{(2)}_{J,K} + \cdots,\\
\hat{u}_{J,K} &= \hat{u}^{(0)}_{J,K} + \varepsilon\hat{u}^{(1)}_{J,K} + \varepsilon^2\hat{u}^{(2)}_{J,K} + \cdots,\\
\hat{v}_{J,K} &= \hat{v}^{(0)}_{J,K} + \varepsilon\hat{v}^{(1)}_{J,K} + \varepsilon^2\hat{v}^{(2)}_{J,K} + \cdots,
\end{aligned} \tag{3.26}$$

where (J,K) is either (j,k), $(j+\frac{1}{2},k)$ or $(j,k+\frac{1}{2})$. Further, at time level $t=t^n$, the computed solution satisfies the following discrete analogs of the asymptotic expansions (2.8) and (2.11):

$$\begin{aligned}
h^n_{j,k} &= h^{(0),n}_{j,k} + \varepsilon h^{(1),n}_{j,k} + \varepsilon^2 h^{(2),n}_{j,k} + \cdots,\\
u^n_{j,k} &= u^{(0),n}_{j,k} + \varepsilon u^{(1),n}_{j,k} + \varepsilon^2 u^{(2),n}_{j,k} + \cdots,\\
v^n_{j,k} &= v^{(0),n}_{j,k} + \varepsilon v^{(1),n}_{j,k} + \varepsilon^2 v^{(2),n}_{j,k} + \cdots,\\
\overline{(h')}^n_{j,k} &= \varepsilon^2(h')^{(2),n}_{j,k} + \cdots,\\
(u')^n_{j,k} &= \varepsilon(u')^{(1),n}_{j,k} + \varepsilon^2(u')^{(2),n}_{j,k} + \cdots,\\
(v')^n_{j,k} &= \varepsilon(v')^{(1),n}_{j,k} + \varepsilon^2(v')^{(2),n}_{j,k} + \cdots,\\
(h')^i_{j,k} &= \varepsilon^2(h')^{i,(2)}_{j,k} + \cdots,\\
(u')^i_{j,k} &= \varepsilon(u')^{i,(1)}_{j,k} + \varepsilon^2(u')^{i,(2)}_{j,k} + \cdots,\\
(v')^i_{j,k} &= \varepsilon(v')^{i,(1)}_{j,k} + \varepsilon^2(v')^{i,(2)}_{j,k} + \cdots,
\end{aligned} \tag{3.27}$$

where $i \in \{\mathrm{E},\mathrm{W},\mathrm{N},\mathrm{S}\}$. We also use the definition of $a(t)$ in (3.5) and the fact that

$$\hat{h}^{(0)} + Z = \text{Const} \tag{3.28}$$

which can be concluded from the first two equations in (2.10), to obtain the following expansion for $a^n = a(t^n)$:

$$a^n = \hat{h}^{(0)} + Z + \varepsilon a^{(1),n} + \varepsilon^2 a^{(2),n} + \cdots, \tag{3.29}$$

where $a^{(1),n}$ and $a^{(2),n}$ are constants.

Proposition 3.3 *Assume that in addition to the asymptotic expansions (3.26)–(3.29), the discrete analogs of the first two equations in (2.15),*

$$(u')^{(1),n}_{j,k} = -D_y(h')^{(2),n}_{j,k} \quad \textit{and} \quad (v')^{(1),n}_{j,k} = D_x(h')^{(2),n}_{j,k},$$

are satisfied for all j,k.

Then the numerical solution at time level $t = t^{n+1}$ can be expanded with respect to ε as follows:

$$\begin{aligned}
\overline{(h')}_{j,k}^{n+1} &= \varepsilon^2 (h')_{j,k}^{(2),n+1} + \cdots, \\
(u')_{j,k}^{n+1} &= \varepsilon (u')_{j,k}^{(1),n+1} + \varepsilon^2 (u')_{j,k}^{(2),n+1} + \cdots, \\
(v')_{j,k}^{n+1} &= \varepsilon (v')_{j,k}^{(1),n+1} + \varepsilon^2 (v')_{j,k}^{(2),n+1} + \cdots,
\end{aligned} \tag{3.30}$$

and the fully discrete scheme provides a consistent approximation of the system (2.15).

Proof: We recall that $1 - \alpha = 1 - \varepsilon^2 = \mathcal{O}(1)$. Using the definitions of $\widetilde{K}$ and K yields

$$\frac{1}{\widetilde{K}} = \left[1 - \left(\frac{\varepsilon}{\Delta t}\right)^2 + \cdots\right] = \mathcal{O}(1), \quad \frac{1}{K} = \left(\frac{\varepsilon}{\Delta t}\right)^2 \left[1 - \left(\frac{\varepsilon}{\Delta t}\right)^2 + \cdots\right] = \mathcal{O}(\varepsilon^2).$$

Moreover, one may easily verify that $\mathcal{R}_{j,k}^{h',n} = \mathcal{O}(\varepsilon^2)$, $\mathcal{R}_{j,k}^{hu,n} = \mathcal{O}(\varepsilon)$ and $\mathcal{R}_{j,k}^{hv,n} = \mathcal{O}(\varepsilon)$.

Equation (3.21) implies that

$$\mathcal{A}\overline{(h')}^{n+1} := \left[I + \frac{1-\alpha}{\widetilde{K}}\Big((Z - a^n)\widetilde{\Delta} + (D_x - \frac{\Delta t}{\varepsilon} D_y) Z D_x + (D_y + \frac{\Delta t}{\varepsilon} D_x) Z D_y\Big)\right] \overline{(h')}^{n+1} = \mathcal{O}(\varepsilon^2),$$

where $\mathcal{A}$ is the linear operator whose corresponding matrix is pentadiagonal and strictly diagonally dominant. Therefore, it is nonsingular (with eigenvalues bounded away from zero independently of ε), and hence the first expansion in equation (3.30) is validated. Using this expansion in equations (3.22) and (3.23) leads to

$$(hu)_{j,k}^{n+1} = \hat{h}_{j,k}\hat{u}_{j,k} + \mathcal{O}(\varepsilon), \quad (hv)_{j,k}^{n+1} = \hat{h}_{j,k}\hat{v}_{j,k} + \mathcal{O}(\varepsilon).$$

This in turn implies the second and the third expansions in (3.30).

Equipped with the established expansions in (3.30), we turn to the asymptotic analysis of the fully discrete WB-AP scheme. To this end we compare ε-like terms. For $\mathcal{O}(\varepsilon)$ terms appearing in (3.22) and (3.23) we obtain

$$(u')_{j,k}^{(1),n+1} = -D_y (h')_{j,k}^{(2),n+1}, \quad (v')_{j,k}^{(1),n+1} = D_x (h')_{j,k}^{(2),n+1}, \tag{3.31}$$

which are consistent discrete approximations of the first two limiting equations in (2.15).

In order to derive the discrete versions of the third and fourth equations in (2.15) we first rewrite equation (3.23) as

$$\begin{aligned}
\big(\hat{h}v' + h'v\big)_{j,k}^n + \Delta t \mathcal{R}_{j,k}^{hv,n} =& K\Big[\overline{(hv)}_{j,k}^{n+1} - \hat{h}_{j,k}\hat{v}_{j,k}\Big] + \frac{\Delta t}{\varepsilon}\big(\hat{h}u' + h'u\big)_{j,k}^n + \frac{(\Delta t)^2}{\varepsilon}\mathcal{R}_{j,k}^{hu,n} \\
&- \frac{(Z_{j,k} - a^n)\Delta t}{\varepsilon^2}\Big(D_y\,\overline{(h')}_{j,k}^{n+1} - \frac{\Delta t}{\varepsilon} D_x\,\overline{(h')}_{j,k}^{n+1}\Big).
\end{aligned} \tag{3.32}$$

Substituting (3.32) into equation (3.22) yields

$$\overline{(hu)}_{j,k}^{n+1} - \hat{h}_{j,k}\hat{u}_{j,k} = \big(\hat{h}u' + h'u\big)_{j,k}^n + \Delta t \mathcal{R}_{j,k}^{hu,n} + \frac{\Delta t}{\varepsilon}\Big(\overline{(hv)}_{j,k}^{n+1} - \hat{h}_{j,k}\hat{v}_{j,k}\Big) + \frac{(Z_{j,k} - a^n)\Delta t}{\varepsilon^2} D_x\,\overline{(h')}_{j,k}^{n+1},$$

which further implies that

$$\frac{\overline{(hu)}_{j,k}^{n+1} - \overline{(hu)}_{j,k}^{n}}{\Delta t} - \mathcal{R}_{j,k}^{hu,n} = \frac{1}{\varepsilon}\Big(\overline{(hv)}_{j,k}^{n+1} - \hat{h}_{j,k}\hat{v}_{j,k}\Big) + \frac{Z_{j,k} - a^n}{\varepsilon^2} D_x\,\overline{(h')}_{j,k}^{n+1}. \tag{3.33}$$

We then substitute (3.16) and (3.31) into (3.33), take into account that $\hat{v}^{(0)}_{j,k} = D_x\hat{h}^{(1)}_{j,k} + \mathcal{O}(\Delta^2_{\max})$ and collect $\mathcal{O}(\varepsilon)$ terms:

$$\begin{aligned}\frac{\hat{h}^{(0)}_{j,k}u^{(1),n+1}_{j,k} - \hat{h}^{(0)}_{j,k}u^{(1),n}_{j,k}}{\Delta t} + 2D_x\Big(\hat{h}^{(0)}_{j,k}\hat{u}^{(0)}_{j,k}(u')^{(1),n}_{j,k}\Big) + D_y\Big(\hat{h}^{(0)}_{j,k}\hat{u}^{(0)}_{j,k}(v')^{(1),n}_{j,k} + \hat{h}^{(0)}_{j,k}(u')^{(1),n}_{j,k}\hat{v}^{(0)}_{j,k}\Big)\\ = \hat{h}^{(0)}_{j,k}(v')^{(2),n+1}_{j,k} + \mathcal{Q}^{hu,(1),n}_{j,k} + D_x\Big[\big(\hat{h}^{(1)}_{j,k} - a^{(1),n}\big)\big((h')^{(2),n+1}_{j,k} - (h')^{(2),n}_{j,k}\big)\Big].\end{aligned} \tag{3.34}$$

Similarly, we can derive

$$\begin{aligned}\frac{\hat{h}^{(0)}_{j,k}v^{(1),n+1}_{j,k} - \hat{h}^{(0)}_{j,k}v^{(1),n}_{j,k}}{\Delta t} + D_x\Big(\hat{h}^{(0)}_{j,k}\hat{u}^{(0)}_{j,k}(v')^{(1),n}_{j,k} + \hat{h}^{(0)}_{j,k}(u')^{(1),n}_{j,k}\hat{v}^{(0)}_{j,k}\Big) + 2D_y\Big(\hat{h}^{(0)}_{j,k}\hat{v}^{(0)}_{j,k}(v')^{(1),n}_{j,k}\Big)\\ = -\hat{h}^{(0)}_{j,k}(u')^{(2),n+1}_{j,k} + \mathcal{Q}^{hv,(1),n}_{j,k} + D_y\Big[\big(\hat{h}^{(1)}_{j,k} - a^{(1),n}\big)\big((h')^{(2),n+1}_{j,k} - (h')^{(2),n}_{j,k}\big)\Big].\end{aligned} \tag{3.35}$$

We note that equations (3.34) and (3.35) are consistent discretizations of the momentum equations, that is, the third and fourth equations in (2.15), respectively. Indeed, the last two terms on the RHSs of (3.34) and (3.35) represent the numerical diffusion: while $\mathcal{Q}^{hu,(1),n}_{j,k}$ and $\mathcal{Q}^{hv,(1),n}_{j,k}$ are $\mathcal{O}(\Delta^2_{\max})$ diffusion expansion coefficients from (3.18), the other two terms are temporal diffusion terms proportional to Δt.

Finally, we derive the equation for $(h')^{(2),n+1}_{j,k}$ by considering $\mathcal{O}(\varepsilon^2)$ terms in equation (3.21). Recalling that $\alpha = \varepsilon^2$, see Section 3.1, we derive

$$\begin{aligned}&(h')^{(2),n+1}_{j,k} - \hat{h}^{(0)}_{j,k}\widetilde{\Delta}(h')^{(2),n+1}_{j,k} + D_xZ_{j,k}D_x(h')^{(2),n+1}_{j,k} + D_yZ_{j,k}D_y(h')^{(2),n+1}_{j,k}\\ &= (h')^{(2),n}_{j,k} - D_x\Big(\hat{h}^{(0)}_{j,k}(v')^{(1),n}_{j,k}\Big) + D_y\Big(\hat{h}^{(0)}_{j,k}(u')^{(1),n}_{j,k}\Big) + 2\Delta tD_xD_y\Big(\hat{h}^{(0)}_{j,k}\hat{v}^{(0)}_{j,k}(v')^{(1),n}_{j,k} - \hat{h}^{(0)}_{j,k}\hat{u}^{(0)}_{j,k}(u')^{(1),n}_{j,k}\Big)\\ &+ \Delta tD^2_x\Big(\hat{h}^{(0)}_{j,k}\hat{u}^{(0)}_{j,k}(v')^{(1),n}_{j,k} + \hat{h}^{(0)}_{j,k}\hat{v}^{(0)}_{j,k}(u')^{(1),n}_{j,k}\Big) - \Delta tD^2_y\Big(\hat{h}^{(0)}_{j,k}\hat{u}^{(0)}_{j,k}(v')^{(1),n}_{j,k} + \hat{h}^{(0)}_{j,k}\hat{v}^{(0)}_{j,k}(u')^{(1),n}_{j,k}\Big)\\ &+ \Delta t\Big(\mathcal{Q}^{h',(2),n}_{j,k} - D_x\mathcal{Q}^{hv,(1),n}_{j,k} + D_y\mathcal{Q}^{hu,(1),n}_{j,k}\Big),\end{aligned}$$

which can be rewritten as

$$\begin{aligned}&\frac{(h')^{(2),n+1}_{j,k} - (h')^{(2),n}_{j,k}}{\Delta t} + \frac{1}{\Delta t}\Big[D_x\hat{h}^{(0)}_{j,k}D_x(h')^{(2),n+1}_{j,k} - D_x\Big(\hat{h}^{(0)}_{j,k}D_x(h')^{(2),n+1}_{j,k}\Big)\\ &+ D_y\hat{h}^{(0)}_{j,k}D_y(h')^{(2),n+1}_{j,k} - D_y\Big(\hat{h}^{(0)}_{j,k}D_y(h')^{(2),n+1}_{j,k}\Big) + D_xZ_{j,k}D_x(h')^{(2),n+1}_{j,k} + D_yZ_{j,k}D_y(h')^{(2),n+1}_{j,k}\Big]\\ &= -\frac{1}{\Delta t}\Big[D_x\Big(\hat{h}^{(0)}_{j,k}(v')^{(1),n}_{j,k}\Big) - D_y\Big(\hat{h}^{(0)}_{j,k}(u')^{(1),n}_{j,k}\Big)\Big] + 2D_xD_y\Big(\hat{h}^{(0)}_{j,k}\hat{v}^{(0)}_{j,k}(v')^{(1),n}_{j,k} - \hat{h}^{(0)}_{j,k}\hat{u}^{(0)}_{j,k}(u')^{(1),n}_{j,k}\Big)\\ &+ D^2_x\Big(\hat{h}^{(0)}_{j,k}\hat{u}^{(0)}_{j,k}(v')^{(1),n}_{j,k} + \hat{h}^{(0)}_{j,k}\hat{v}^{(0)}_{j,k}(u')^{(1),n}_{j,k}\Big) - D^2_y\Big(\hat{h}^{(0)}_{j,k}\hat{u}^{(0)}_{j,k}(v')^{(1),n}_{j,k} + \hat{h}^{(0)}_{j,k}\hat{v}^{(0)}_{j,k}(u')^{(1),n}_{j,k}\Big)\\ &+ \mathcal{Q}^{h',(2),n}_{j,k} - D_x\mathcal{Q}^{hv,(1),n}_{j,k} + D_y\mathcal{Q}^{hu,(1),n}_{j,k}.\end{aligned} \tag{3.36}$$

We then substitute (3.28) and (3.31) into equation (3.36) and obtain

$$\begin{aligned}
&\frac{(h')_{j,k}^{(2),n+1}-(h')_{j,k}^{(2),n}}{\Delta t}-\frac{D_x\Big(\hat{h}_{j,k}^{(0)}(v')_{j,k}^{(1),n+1}-\hat{h}_{j,k}^{(0)}(v')_{j,k}^{(1),n}\Big)}{\Delta t}\\
&+\frac{D_y\Big(\hat{h}_{j,k}^{(0)}(u')_{j,k}^{(1),n+1}-\hat{h}_{j,k}^{(0)}(u')_{j,k}^{(1),n}\Big)}{\Delta t}=2D_xD_y\Big(\hat{h}_{j,k}^{(0)}\hat{v}_{j,k}^{(0)}(v')_{j,k}^{(1),n}-\hat{h}_{j,k}^{(0)}\hat{u}_{j,k}^{(0)}(u')_{j,k}^{(1),n}\Big)\\
&+D_x^2\Big(\hat{h}_{j,k}^{(0)}\hat{u}_{j,k}^{(0)}(v')_{j,k}^{(1),n}+\hat{h}_{j,k}^{(0)}\hat{v}_{j,k}^{(0)}(u')_{j,k}^{(1),n}\Big)-D_y^2\Big(\hat{h}_{j,k}^{(0)}\hat{u}_{j,k}^{(0)}(v')_{j,k}^{(1),n}+\hat{h}_{j,k}^{(0)}\hat{v}_{j,k}^{(0)}(u')_{j,k}^{(1),n}\Big)\\
&+\mathcal{Q}_{j,k}^{h',(2),n}-D_x\mathcal{Q}_{j,k}^{hv,(1),n}+D_y\mathcal{Q}_{j,k}^{hu,(1),n},
\end{aligned}\tag{3.37}$$

which is a consistent discretization of the mass equation, that is, the last equation in (2.15). Note that the last three terms on the RHS of (3.37) are $\mathcal{O}(\Delta_{\max}^2)$ diffusion expansion coefficients from (3.18).

In summary, the proposed numerical scheme yields the discrete limiting equations (3.31), (3.34), (3.35) and (3.37), which are consistent approximations of the system (2.15). ■

4 Numerical Examples

In this section we demonstrate the performance of the proposed WB-AP scheme on a number of numerical examples. In what follows we refer to our new WB-AP scheme as the NEW scheme. The obtained results are compared with those computed by the the non-WB AP scheme from [32], which will be referred to as the OLD scheme.

The time step is adaptively determined using the CFL condition for the nonstiff hyperbolic system. We set the CFL number to be 0.2, namely, we take

$$\Delta t=0.2\min\left\{\frac{\Delta x}{a_{\max}},\frac{\Delta y}{b_{\max}}\right\},$$

where

$$a_{\max}:=\max_{j,k}\left\{\max\left(a^+_{j+\frac12,k},-a^-_{j+\frac12,k}\right)\right\},\quad b_{\max}:=\max_{j,k}\left\{\max\left(b^+_{j,k+\frac12},-b^-_{j,k+\frac12}\right)\right\},$$

and $a^{\pm}_{j+\frac12,k}$ and $b^{\pm}_{j,k+\frac12}$ are defined in (3.13).

In all of the examples below the computational domain $[-1,1]\times[-1,1]$ has been covered by an 80×80 uniform mesh (in the second part of Example 3, we also use a finer 480×480 uniform mesh). We use free boundary conditions in both the x- and y-directions.

Discrete Steady Velocity Fields Correction

Before conducting the numerical experiments, we would like to point out at the necessity of preparing the steady velocity field, which should satisfy the condition (2.3a) at the discrete level. To this end, we first notice that (2.3a) implies that there exists a potential ψ such that

$$\hat{h}\hat{u}=\psi_y,\quad \hat{h}\hat{v}=-\psi_x,$$

which, in turn, gives the following elliptic equation for ψ:

$$\Delta\psi = -(\hat{h}\hat{v})_x + (\hat{h}\hat{u})_y. \tag{4.1}$$

We then discretize equation (4.1) using the standard central differences,

$$\widetilde{\Delta}\psi_{j,k} = -D_x\big(\hat{h}_{j,k}\hat{v}_{j,k}\big) + D_y\big(\hat{h}_{j,k}\hat{u}_{j,k}\big), \tag{4.2}$$

and solve the linear algebraic system (4.2) for $\psi_{j,k}$. Note that the discrete quantities on the RHS of (4.2) are given by $\hat{h}_{j,k} := \hat{h}(x_j, y_k)$, $\hat{u}_{j,k} := \hat{u}(x_j, y_k)$ and $\hat{v}_{j,k} := \hat{v}(x_j, y_k)$.

Once $\big\{\psi_{j,k}\big\}$ are available, we replace $\hat{u}_{j,k}$ and $\hat{v}_{j,k}$ with the following modified discrete steady velocities:

$$\hat{\hat{u}}_{j,k} = \frac{D_y\psi_{j,k}}{\hat{h}_{j,k}}, \quad \hat{\hat{v}}_{j,k} = -\frac{D_x\psi_{j,k}}{\hat{h}_{j,k}},$$

which clearly satisfy the following discrete analogue of (2.3a):

$$D_x\big(\hat{h}_{j,k}\hat{\hat{u}}_{j,k}\big) + D_y\big(\hat{h}_{j,k}\hat{\hat{v}}_{j,k}\big) = 0.$$

Example 1—Stationary Vortex with $\mathcal{O}(\varepsilon)$ Velocity Fields

In this example we consider a stationary vortex described by the following initial conditions:

$$h(r,0) = 1 + \varepsilon^2\begin{cases}\dfrac{5}{2}(1+5\varepsilon^2)r^2, & r \leqslant \dfrac{1}{5}\\[2ex] \dfrac{1}{10}(1+5\varepsilon^2) + 2r - \dfrac{3}{10} - \dfrac{5}{2}r^2 + \varepsilon^2\left[4\ln(5r) + \dfrac{7}{2} - 20r + \dfrac{25}{2}r^2\right], & \dfrac{1}{5} < r < \dfrac{2}{5},\\[2ex] \dfrac{1}{5}(1 - 10\varepsilon^2 + 20\varepsilon^2\ln 2), & r \geqslant \dfrac{2}{5},\end{cases}$$

$$u(x,y,0) = -\varepsilon y\gamma(r), \quad v(x,y,0) = \varepsilon x\gamma(r), \quad \gamma(r) := \begin{cases}5, & r \leqslant \dfrac{1}{5},\\[2ex] \dfrac{2}{r} - 5, & \dfrac{1}{5} < r < \dfrac{2}{5},\\[2ex] 0, & r \geqslant \dfrac{2}{5},\end{cases}$$

where $r := \sqrt{x^2+y^2}$. The bottom topography is flat and $Z(x,y) \equiv 0$.

We begin with the large Froude number $\varepsilon = 1$ and compute the solutions until the final time $t = 80$. The snapshots of h at $t = 10$, 50 and 80 computed by the NEW and OLD schemes are shown in Figure 4.1. As one can clearly see, the numerical solution computed by the OLD scheme significantly dissipates in time, while the NEW scheme preserves the initial solution shape of h. This demonstrates the importance of the WB property of the NEW scheme.

We proceed by testing both schemes in the cases of small Froude numbers $\varepsilon = 10^{-p}$ for $p = 1$, 2, 3 and 4. We run the simulations until the final times $t = 160$, 240, 320 and 480, respectively. In Figures 4.2–4.5, we plot the water depth h at different times. These results show that the NEW scheme clearly outperforms the OLD one for a wide range of ε.

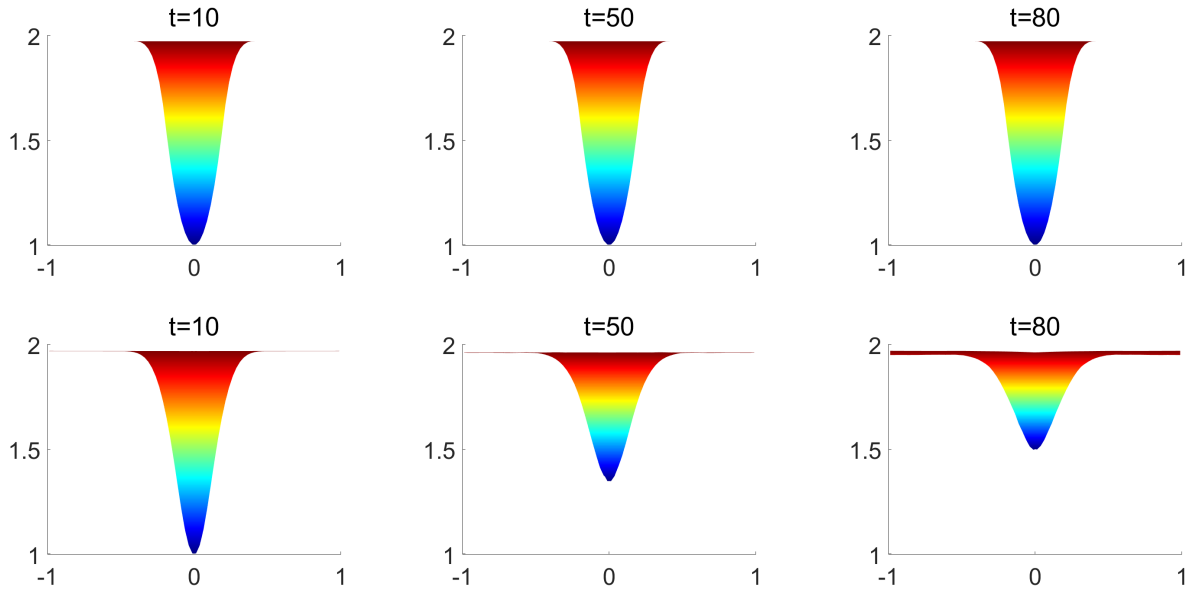

Figure 4.1: Example 1: Front view of h for $\varepsilon = 1$ computed by the NEW (top row) and OLD (bottom row) schemes.

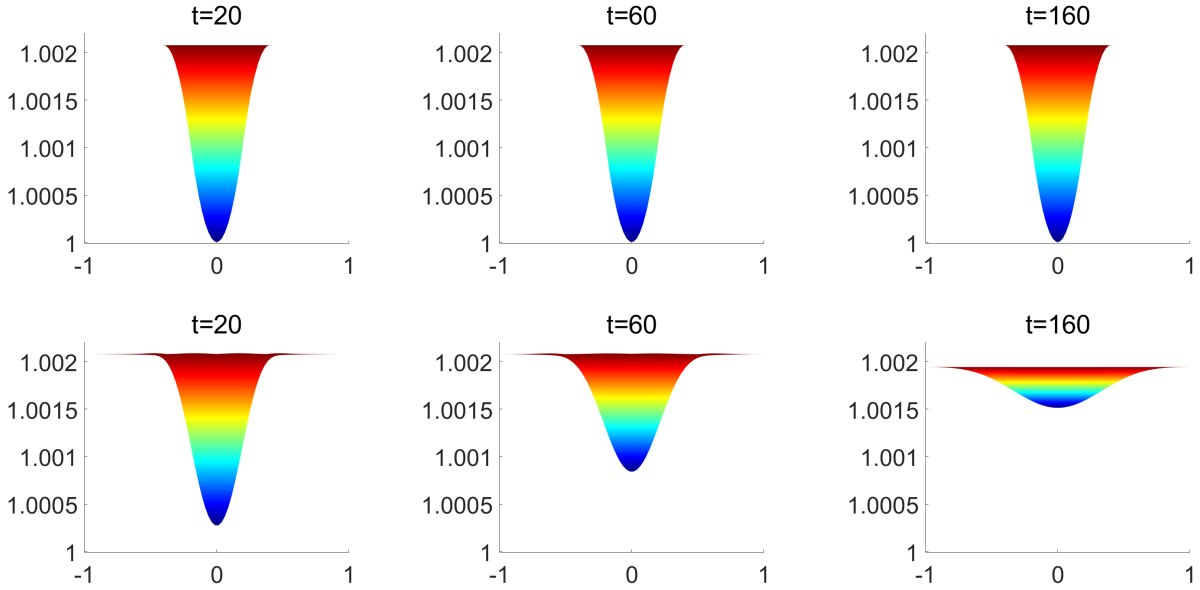

Figure 4.2: Example 1: The same as Figure 4.1, but for $\varepsilon = 10^{-1}$.

Example 2—Stationary Vortex with $\mathcal{O}(1)$ Velocity Fields

In this example we consider another stationary vortex, which can be described by the following initial data:

$$h(r,0) = 1 + \varepsilon \begin{cases} \dfrac{5}{2}(1+5\varepsilon)r^2, & r \leqslant \dfrac{1}{5} \\ \dfrac{1}{10}(1+5\varepsilon) + 2r - \dfrac{3}{10} - \dfrac{5}{2}r^2 + \varepsilon\left[4\ln(5r) + \dfrac{7}{2} - 20r + \dfrac{25}{2}r^2\right], & \dfrac{1}{5} < r < \dfrac{2}{5}, \\ \dfrac{1}{5}(1 - 10\varepsilon + 20\varepsilon\ln 2), & r \geqslant \dfrac{2}{5}, \end{cases}$$

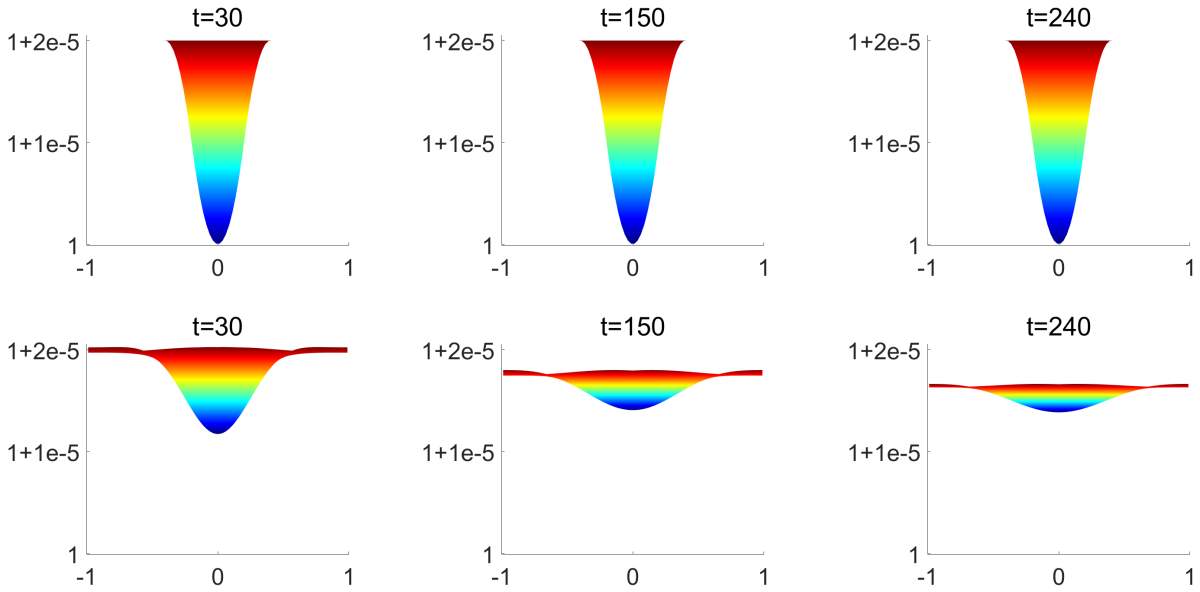

Figure 4.3: Example 1: The same as Figure 4.1, but for $\varepsilon = 10^{-2}$.

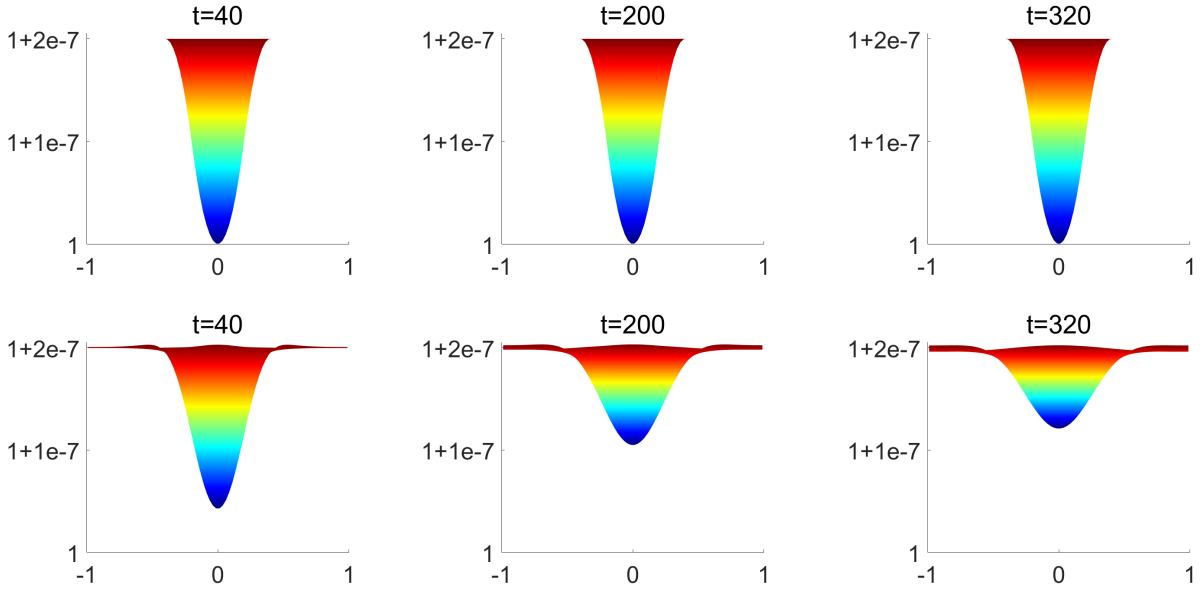

Figure 4.4: Example 1: The same as Figure 4.1, but for $\varepsilon = 10^{-3}$.

$$u(x,y,0) = -y\gamma(r), \quad v(x,y,0) = x\gamma(r), \quad \gamma(r) := \begin{cases} 5, & r \leqslant \dfrac{1}{5}, \\ \dfrac{2}{r} - 5, & \dfrac{1}{5} < r < \dfrac{2}{5}, \\ 0, & r \geqslant \dfrac{2}{5}. \end{cases}$$

The bottom topography is flat and $Z(x,y) \equiv 0$.

We note that even though the initial conditions in Examples 1 and 2 are similar, the scaling in

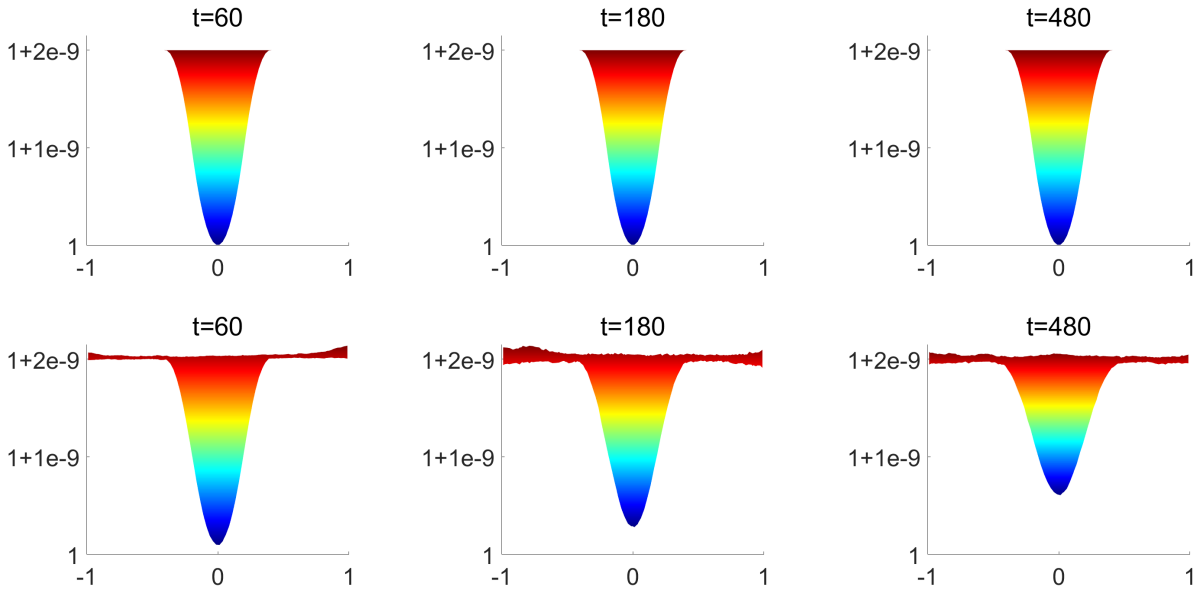

Figure 4.5: The same as Figure 4.1, but for $\varepsilon = 10^{-4}$.

the current example makes the problem computationally more challenging. As $\varepsilon \to 0$, the steady state in Example 1 approaches a "lake at rest" equilibrium, while in the present test the magnitude of the velicities remains $\mathcal{O}(1)$. Moreover, we need to exactly resolve a "moving water" equilibria. Figures 4.6–4.8, where we plot time evolution of h computed by the NEW and OLD schemes at $t = 10$, 30 and 60 for $\varepsilon = 10^{-1}$, 10^{-2} and 10^{-4} show that the NEW scheme still accurately preserves the structure of the vortex and its advantage over the OLD scheme is now even more pronounced than in Example 1.

Example 3—Small Perturbation of a Stationary Vortex over a Nonflat Bottom

In the final example we test the ability of the proposed WB-AP scheme to accurately capture a small perturbation of a stationary vortex and to handle a nonflat bottom topography.

We first consider a stationary vortex with

$$w(r,0) = 1 + \varepsilon \begin{cases} \dfrac{5}{2}(1+5\varepsilon)r^2, & r \leqslant \dfrac{1}{5} \\ \dfrac{1}{10}(1+5\varepsilon) + 2r - \dfrac{3}{10} - \dfrac{5}{2}r^2 + \varepsilon\left[4\ln(5r) + \dfrac{7}{2} - 20r + \dfrac{25}{2}r^2\right], & \dfrac{1}{5} < r < \dfrac{2}{5}, \\ \dfrac{1}{5}(1 - 10\varepsilon + 20\varepsilon\ln 2), & r \geqslant \dfrac{2}{5}, \end{cases}$$

where $w(r,0) = h(r,0) + Z(x,y)$ and the bottom topography consists of an elliptical shaped hump:

$$Z(x,y) = \frac{1}{2}e^{-20\left[(x+0.1)^2+y^2\right]}.$$

The initial velocities $u(x,y,0)$ and $v(x,y,0)$ are the same as in Example 2.

We compute the numerical solution for $\varepsilon = 10^{-2}$ until the final time $t = 60$. We plot the snapshots (at $t = 10$, 30 and 60) of the computed solutions ($w = h + Z$ and h) in Figures 4.9

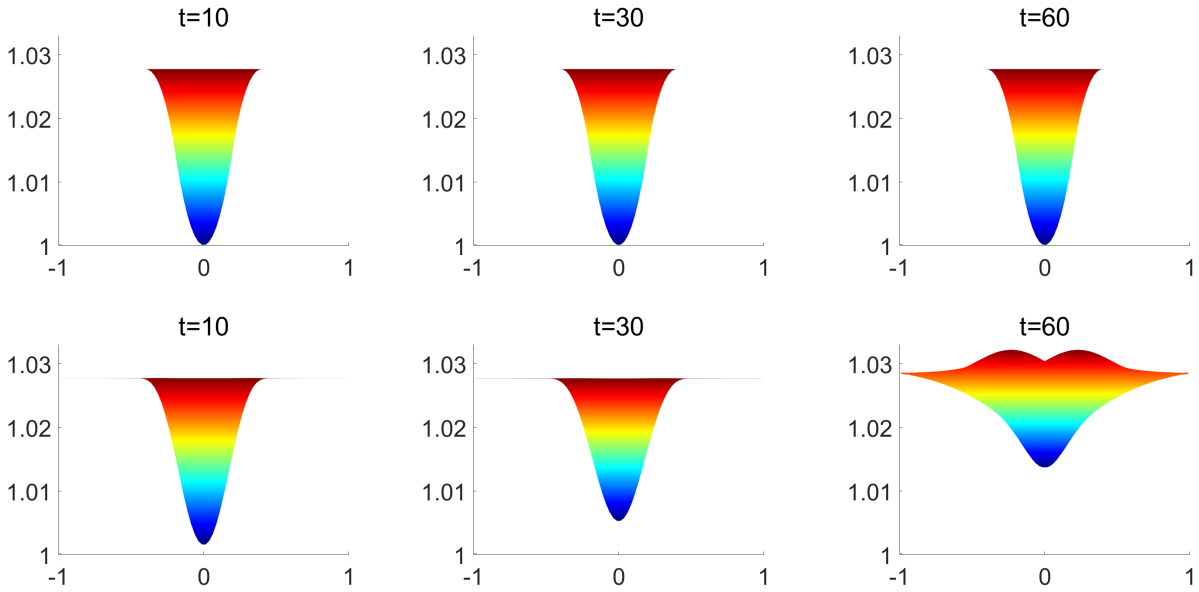

Figure 4.6: Example 2: Front view of h for $\varepsilon = 10^{-1}$ computed by the NEW (top row) and OLD (bottom row) schemes.

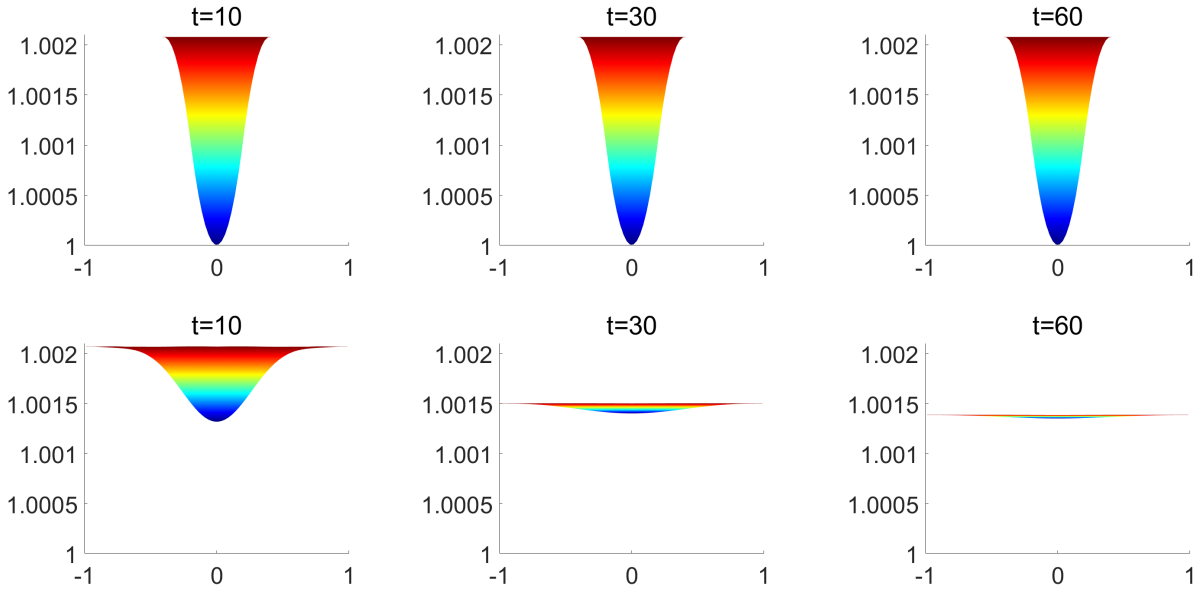

Figure 4.7: Example 2: The same as Figure 4.6, but for $\varepsilon = 10^{-2}$.

and 4.10, respectively. As one can see, the proposed WB-AP scheme is capable of preserving the stationary vortex over the nonflat bottom topography.

Finally, we superimpose a small perturbation around the core of the vortex onto the initial water surface by replacing $w(r,0)$ with

$$\widetilde{w}(r,0) = w(r,0) + \begin{cases} 10^{-4}, & 0.04 < r < 0.16, \\ 0, & \text{otherwise.} \end{cases}$$

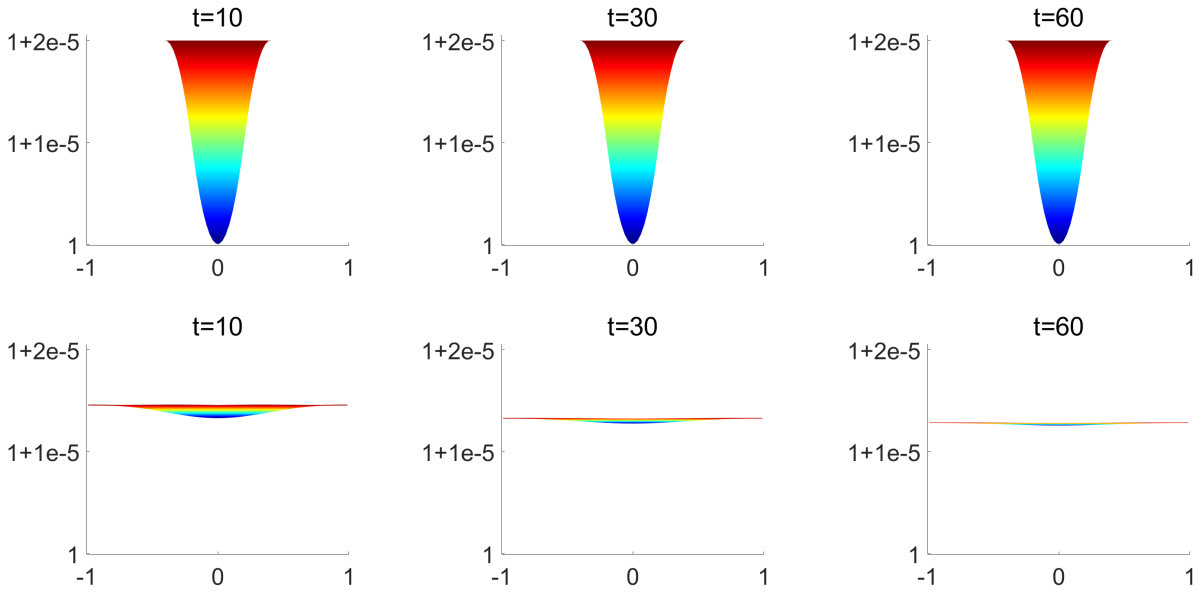

Figure 4.8: Example 2: The same as Figure 4.6, but for $\varepsilon = 10^{-4}$.

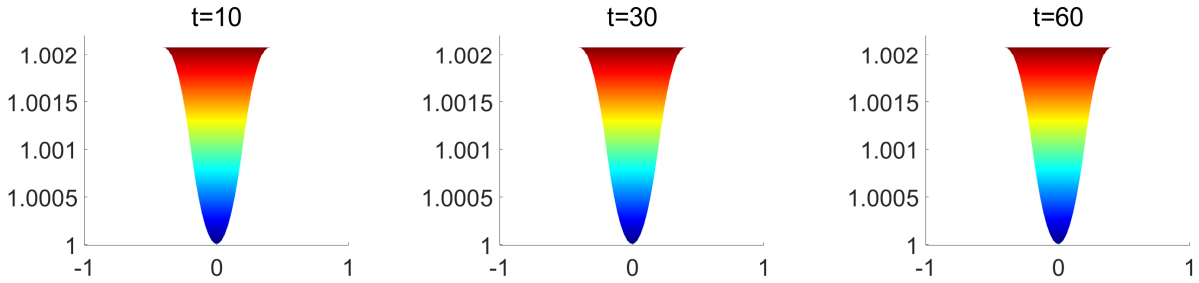

Figure 4.9: Example 3: Front view of $w = h + Z$ computed by the NEW scheme.

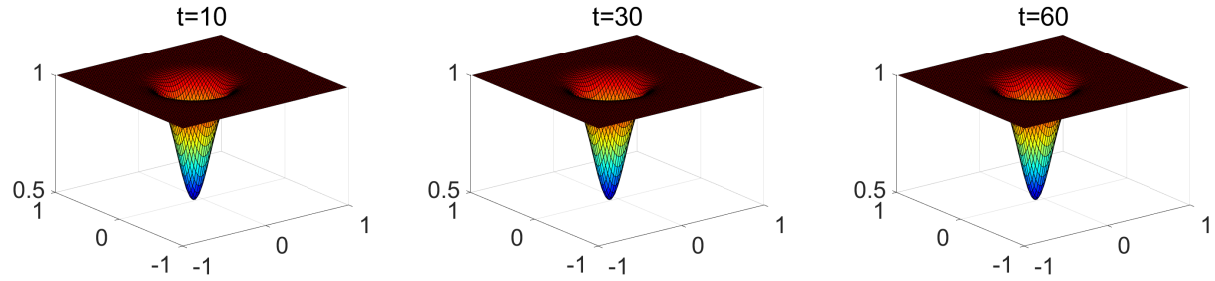

Figure 4.10: Example 3 (stationary vortex): h computed by the NEW scheme.

In Figure 4.11 (left column), the water surface w, computed by the NEW scheme on the coarse (80×80) and fine (480×480) meshes, are presented at the final time $t = 0.002$.

In order to demonstrate the importance of the WB property we also compute the solutions on the same meshes using the OLD scheme. The non-WB solutions are shown in the right column of Figure 4.11. As one can clearly see, the solutions computed by the OLD scheme contain spurious waves, not present in the solutions computed by the NEW scheme even when the coarse 80×80

mesh is used. In order to better see the waves generated by the small perturbation, we plot the difference between the computed w and the background equilibrium $w(r,0)$; see Figure 4.12. Once again, we observe that while the NEW scheme captures the propagating perturbation in a clrealy non-oscillatory manner and the resolution, as expected, increases when the mesh is refined (see the left column of Figure 4.12), the results computed by the non-WB OLD scheme are unsatisfactory even when the fine 480×480 mesh is used. Indeed, as one can see in the right column of Figure 4.12, the magnitude of the artificial waves is substantially larger than the magnitude of the perturbation to be computed. This clearly indicates the advantage of the WB NEW scheme over the non-WB OLD one.

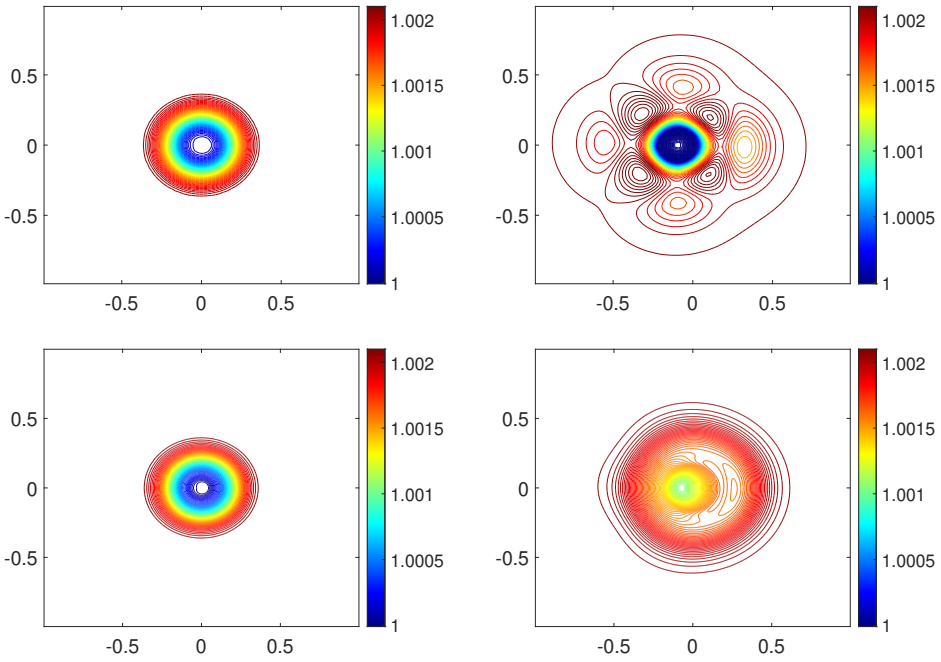

Figure 4.11: Example 3 (small Perturbation of a stationary vortex): w computed by the NEW (left column) and OLD (right column) schemes using the coarse 80×80 (top row) and fine 480×480 (bottom row) meshes.

Acknowledgment

The work of A. Kurganov was supported in part by NSFC grants 11771201 and 1201101343, and by the fund of the Guangdong Provincial Key Laboratory of Computational Science and Material Design (No. 2019B030301001). The work of M. Lukáčová-Medviďová was supported in part by the German Science Foundation under the Collaborative Research Center TRR 165 Waves to Weather (Project A2). M. Lukáčová-Medviďová also gratefully acknowledges the Gutenberg Research College for supporting her research.

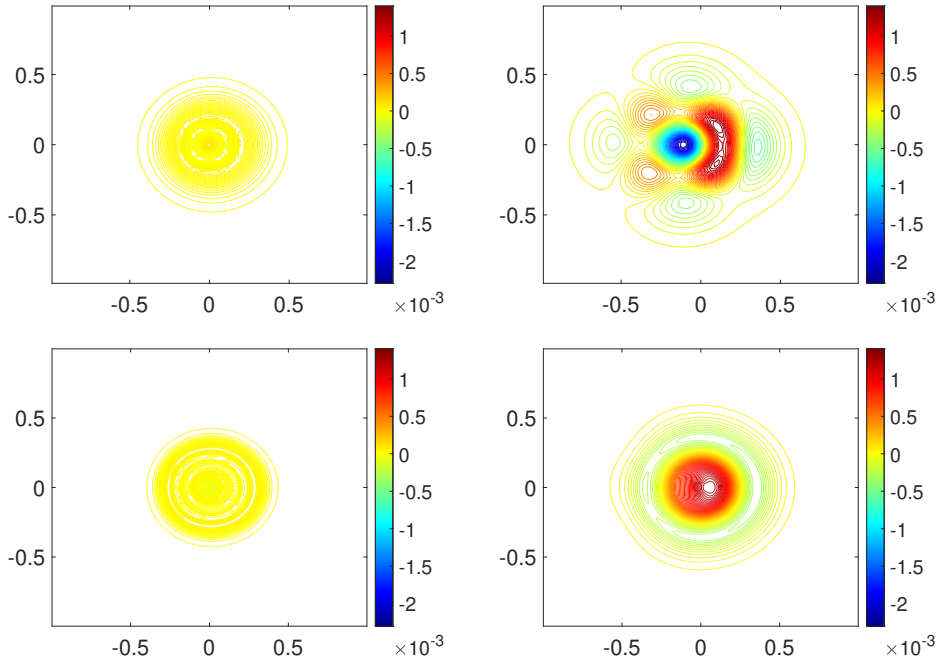

Figure 4.12: Example 3 (small perturbation of a stationary vortex): $w-w(r,0)$ computed by the NEW (left column) and OLD (right column) schemes using the coarse 80×80 (top row) and fine 480×480 (bottom row) meshes.

A Asymptotic Expansions of the Numerical Diffusion Terms

In this section we follow the approach used in [32] to investigate the leading order of the numerical diffusion (3.15). Without loss of generality, we only consider the numerical diffusion of the x-direction given by (3.15a), and expand the unknowns there using the asymptotic expansions given by (3.26) and (3.27).

Then the leading order approximation of the first component of the numerical diffusion in (3.15a) reads as

$$\mathcal{D}^{h',n}_{j+\frac12,k}=\alpha\varepsilon\left(\hat h^{(0)}_{j+\frac12,k}\frac{a^+_{j+\frac12,k}(u')^{\mathrm{E},(1)}_{j,k}-a^-_{j+\frac12,k}(u')^{\mathrm{W},(1)}_{j+1,k}}{a^+_{j+\frac12,k}-a^-_{j+\frac12,k}}-\frac{\hat h^{(0)}_{j,k}(u')^{(1),n}_{j,k}+\hat h^{(0)}_{j+1,k}(u')^{(1),n}_{j+1,k}}{2}\right)$$
$$+\frac{\varepsilon^2a^+_{j+\frac12,k}a^-_{j+\frac12,k}}{a^+_{j+\frac12,k}-a^-_{j+\frac12,k}}\left((h')^{\mathrm{W},(2)}_{j+1,k}-(h')^{\mathrm{E},(2)}_{j,k}\right),$$

which consequently implies that the leading order of $\mathcal{D}^{h',n}_{j+\frac12,k}$ is $\mathcal{O}(\varepsilon^2)$ as $\alpha=\varepsilon^s$, where $s\geqslant1$; see Section 3.1.

For the second and third components of the numerical diffusion (3.15a) we have

$$\begin{aligned}\mathcal{D}^{hu,n}_{j+\frac12,k} &= 2\varepsilon\hat h^{(0)}_{j+\frac12,k}\hat u^{(0)}_{j+\frac12,k}\frac{a^+_{j+\frac12,k}(u')^{\mathrm{E},(1)}_{j,k}-a^-_{j+\frac12,k}(u')^{\mathrm{W},(1)}_{j+1,k}}{a^+_{j+\frac12,k}-a^-_{j+\frac12,k}}+\varepsilon a^{(1),n}\frac{a^+_{j+\frac12,k}(h')^{\mathrm{E},(2)}_{j,k}-a^-_{j+\frac12,k}(h')^{\mathrm{W},(2)}_{j+1,k}}{a^+_{j+\frac12,k}-a^-_{j+\frac12,k}}\\ &\quad-\varepsilon\left(\hat h^{(0)}_{j,k}\hat u^{(0)}_{j,k}(u')^{(1),n}_{j,k}+\hat h^{(0)}_{j+1,k}\hat u^{(0)}_{j+1,k}(u')^{(1),n}_{j+1,k}\right)-\varepsilon a^{(1),n}\frac{(h')^{(2),n}_{j,k}+(h')^{(2),n}_{j+1,k}}{2}\\ &\quad+\frac{\varepsilon a^+_{j+\frac12,k}a^-_{j+\frac12,k}}{a^+_{j+\frac12,k}-a^-_{j+\frac12,k}}\hat h^{(0)}_{j+\frac12,k}\left((u')^{\mathrm{W},(1)}_{j+1,k}-(u')^{\mathrm{E},(1)}_{j,k}\right)+\mathcal{O}(\varepsilon^2)\end{aligned}$$

and

$$\begin{aligned}\mathcal{D}^{hv,n}_{j+\frac12,k} &= \varepsilon\hat h^{(0)}_{j+\frac12,k}\left(\hat u^{(0)}_{j+\frac12,k}\frac{a^+_{j+\frac12,k}(v')^{\mathrm{E},(1)}_{j,k}-a^-_{j+\frac12,k}(v')^{\mathrm{W},(1)}_{j+1,k}}{a^+_{j+\frac12,k}-a^-_{j+\frac12,k}}+\hat v^{(0)}_{j+\frac12,k}\frac{a^+_{j+\frac12,k}(u')^{\mathrm{E},(1)}_{j,k}-a^-_{j+\frac12,k}(u')^{\mathrm{W},(1)}_{j+1,k}}{a^+_{j+\frac12,k}-a^-_{j+\frac12,k}}\right)\\ &\quad-\frac{\varepsilon}{2}\left[\hat h^{(0)}_{j,k}\left(\hat u^{(0)}_{j,k}(v')^{(1),n}_{j,k}+\hat v^{(0)}_{j,k}(u')^{(1),n}_{j,k}\right)+\hat h^{(0)}_{j+1,k}\left(\hat u^{(0)}_{j+1,k}(v')^{(1),n}_{j+1,k}+\hat v^{(0)}_{j+1,k}(u')^{(1),n}_{j+1,k}\right)\right]\\ &\quad+\frac{\varepsilon a^+_{j+\frac12,k}a^-_{j+\frac12,k}}{a^+_{j+\frac12,k}-a^-_{j+\frac12,k}}\hat h^{(0)}_{j+\frac12,k}\left((v')^{\mathrm{W},(1)}_{j+1,k}-(v')^{\mathrm{E},(1)}_{j,k}\right)+\mathcal{O}(\varepsilon^2).\end{aligned}$$

Consequently, the leading order of both $\mathcal{D}^{hu,n}_{j+\frac12,k}$ and $\mathcal{D}^{hv,n}_{j+\frac12,k}$ is $\mathcal{O}(\varepsilon)$.

B Second-Order IMEX Fully Discrete WB-AP Scheme

In this section we describe how to increase the temporal order of accuracy of the presented WB-AP scheme by implementing the second-order two-stage IMEX Runge-Kutta ARS(2,2,2) method.

The first stage of the ARS(2,2,2) method applied to the system (3.1) can be written as

$$\begin{aligned}&\frac{(h')^*-(h')^n}{\Delta t}+\gamma\alpha\left[(hu'+h'\hat u)^n_x+(hv'+h'\hat v)^n_y\right]+\gamma(1-\alpha)\left[(hu)^*_x+(hv)^*_y\right]=0,\\ &\frac{(hu)^*-(hu)^n}{\Delta t}+\gamma\left(2\hat h\hat u u'+\hat h(u')^2+h'u^2+\frac{\frac{(h')^2}{2}+\big(\hat h+Z-a(t)\big)h'}{\varepsilon^2}\right)^n_x\\ &\qquad+\gamma\big(\hat h\hat u v'+\hat h u'v+h'uv\big)^n_y+\frac{\gamma a(t)}{\varepsilon^2}(h')^*_x=\frac{\gamma}{\varepsilon}(hv)^*-\frac{\gamma}{\varepsilon}\hat h\hat v+\frac{\gamma}{\varepsilon^2}(h')^*_xZ,\qquad\text{(B.1)}\\ &\frac{(hv)^*-(hv)^n}{\Delta t}+\gamma\left(2\hat h\hat v v'+\hat h(v')^2+h'v^2+\frac{\frac{(h')^2}{2}+\big(\hat h+Z-a(t)\big)h'}{\varepsilon^2}\right)^n_y\\ &\qquad+\gamma\big(\hat h\hat u v'+\hat h u'v+h'uv\big)^n_x+\frac{\gamma a(t)}{\varepsilon^2}(h')^*_y=-\frac{\gamma}{\varepsilon}(hu)^*+\frac{\gamma}{\varepsilon}\hat h\hat u+\frac{\gamma}{\varepsilon^2}(h')^*_yZ,\end{aligned}$$

where $(\cdot)^*$ is used to denote the quantities computed at the first stage. We notice that the system (B.1) coincides with the system (3.6) with Δt replaced with $\tau:=\gamma\Delta t$. Therefore, we obtain the

following equations (similar to (3.21)–(3.23)) for $(h')^*$, $(hu)^*$ and $(hv)^*$:

$$
\begin{aligned}
&\overline{(h')}^*_{j,k} + \frac{(Z_{j,k}-a^n)(1-\alpha)}{\widetilde{K}_\tau}\widetilde{\Delta}\,\overline{(h')}^*_{j,k}\\
&\quad + \frac{1-\alpha}{\widetilde{K}_\tau}\Big[\Big(D_x - \frac{\tau}{\varepsilon}D_y\Big)Z_{j,k}D_x\,\overline{(h')}^*_{j,k} + \Big(D_y + \frac{\tau}{\varepsilon}D_x\Big)Z_{j,k}D_y\,\overline{(h')}^*_{j,k}\Big]\\
&\quad = \overline{(h')}^n_{j,k} + \tau\mathcal{R}^{h',n}_{j,k} - \frac{\Delta t(1-\alpha)}{K_\tau}\Big[D_x(\hat{h}u'+h'u)^n_{j,k} + D_y(\hat{h}v'+h'v)^n_{j,k}\\
&\quad + \frac{\tau}{\varepsilon}\Big(D_x(\hat{h}v'+h'v)^n_{j,k} - D_y(\hat{h}u'+h'u)^n_{j,k}\Big)\\
&\quad + \tau\left(D_x\mathcal{R}^{hu,n}_{j,k} + D_y\mathcal{R}^{hv,n}_{j,k}\right) + \frac{\tau^2}{\varepsilon}\left(D_x\mathcal{R}^{hv,n}_{j,k} - D_y\mathcal{R}^{hu,n}_{j,k}\right)\Big],\\
&\overline{(hu)}^*_{j,k} = \hat{h}_{j,k}\hat{u}_{j,k} + \frac{1}{K_\tau}\Big[\big(\hat{h}u'+h'u\big)^n_{j,k} + \frac{\tau}{\varepsilon}\big(\hat{h}v'+h'v\big)^n_{j,k} + \tau\Big(\mathcal{R}^{hu,n}_{j,k} + \frac{\tau}{\varepsilon}\mathcal{R}^{hv,n}_{j,k}\Big)\\
&\quad + \frac{(Z_{j,k}-a^n)\tau}{\varepsilon^2}\Big(D_x\,\overline{(h')}^*_{j,k} + \frac{\Delta t}{\varepsilon}D_y\,\overline{(h')}^*_{j,k}\Big)\Big],\\
&\overline{(hv)}^*_{j,k} = \hat{h}_{j,k}\hat{v}_{j,k} + \frac{1}{K_\tau}\Big[\big(\hat{h}v'+h'v\big)^n_{j,k} - \frac{\tau}{\varepsilon}\big(\hat{h}u'+h'u\big)^n_{j,k} + \tau\Big(\mathcal{R}^{hv,n}_{j,k} - \frac{\tau}{\varepsilon}\mathcal{R}^{hu,n}_{j,k}\Big)\\
&\quad + \frac{(Z_{j,k}-a^n)\tau}{\varepsilon^2}\Big(D_y\,\overline{(h')}^*_{j,k} - \frac{\tau}{\varepsilon}D_x\,\overline{(h')}^*_{j,k}\Big)\Big],
\end{aligned}
$$

where $\widetilde{K}_\tau := 1 + (\varepsilon/\tau)^2$ and $K_\tau := 1 + (\tau/\varepsilon)^2$.

We then proceed with the second stage of the ARS(2,2,2) method, which gives

$$
\begin{aligned}
&\frac{(h')^{n+1}-(h')^n}{\Delta t} + \gamma(1-\alpha)\left[(hu)^{n+1}_x + (hv)^{n+1}_y\right] + (1-\gamma)(1-\alpha)\left[(hu)^*_x + (hv)^*_y\right]\\
&\qquad = \frac{1}{2\gamma}R^{h',*} + \Big(1-\frac{1}{2\gamma}\Big)R^{h',n}, \qquad \text{(B.2a)}\\
&\frac{(hu)^{n+1}-(hu)^n}{\Delta t} + \frac{\gamma a^*}{\varepsilon^2}(h')^{n+1}_x + \frac{(1-\gamma)a^n}{\varepsilon^2}(h)'^*_x - \frac{\gamma}{\varepsilon}(hv)^{n+1} - \frac{1-\gamma}{\varepsilon}(hv)^* + \frac{1}{\varepsilon}\hat{h}\hat{v}\\
&\qquad = \frac{1}{2\gamma}R^{hu,*} + \Big(1-\frac{1}{2\gamma}\Big)R^{hu,n} + \frac{\gamma}{\varepsilon}(h')^{n+1}_x Z + \frac{1-\gamma}{\varepsilon}(h')^*_x Z, \qquad \text{(B.2b)}\\
&\frac{(hv)^{n+1}-(hv)^n}{\Delta t} + \frac{\gamma a^*}{\varepsilon^2}(h')^{n+1}_y + \frac{(1-\gamma)a^n}{\varepsilon^2}(h')^*_y + \frac{\gamma}{\varepsilon}(hu)^{n+1} + \frac{1-\gamma}{\varepsilon}(hu)^* - \frac{1}{\varepsilon}\hat{h}\hat{u}\\
&\qquad = \frac{1}{2\gamma}R^{hv,*} + \Big(1-\frac{1}{2\gamma}\Big)R^{hv,n} + \frac{\gamma}{\varepsilon}(h')^{n+1}_y Z + \frac{1-\gamma}{\varepsilon}(h')^*_y Z. \qquad \text{(B.2c)}
\end{aligned}
$$

Next, we solve equations (B.2b) and (B.2c) for $(hu)^{n+1}$ and $(hv)^{n+1}$ to obtain

$$
\begin{aligned}
(hu)^{n+1} &= \hat{h}\hat{u} + \frac{1}{K_\tau}\Big\{\hat{h}(u')^n + (h'u)^n + \frac{\tau}{\varepsilon}\big(\hat{h}(v')^n + (h'v)^n\big) + \frac{(Z-a^*)\tau}{\varepsilon^2}\Big((h')^{n+1}_x + \frac{\tau}{\varepsilon}(h')^{n+1}_y\Big)\\
&\quad + \frac{\Delta t-\tau}{\varepsilon}\left[\hat{h}(v')^* + (h'v)^* - \frac{\tau}{\varepsilon}\big(\hat{h}(u')^* + (h'u)^*\big) + \frac{Z-a^n}{\varepsilon}\Big((h')^*_x + \frac{\tau}{\varepsilon}(h')^*_y\Big)\right] \qquad \text{(B.3a)}\\
&\quad + \frac{\Delta t}{2\gamma}\left(R^{hu,*} + \frac{\tau}{\varepsilon}R^{hv,*}\right) + \Delta t\Big(1-\frac{1}{2\gamma}\Big)\left(R^{hu,n} + \frac{\tau}{\varepsilon}R^{hv,n}\right)\Big\}\\
(hv)^{n+1} &= \hat{h}\hat{v} + \frac{1}{K_\tau}\Big\{\hat{h}(v')^n + (h'v)^n - \frac{\tau}{\varepsilon}\big(\hat{h}(u')^n + (h'u)^n\big) + \frac{(Z-a^*)\tau}{\varepsilon^2}\Big((h')^{n+1}_y - \frac{\tau}{\varepsilon}(h')^{n+1}_x\Big)
\end{aligned}
$$

$$- \frac{\Delta t-\tau}{\varepsilon}\left[\hat{h}(u')^* + (h'u)^* + \frac{\tau}{\varepsilon}\Big(\hat{h}(v')^* + (h'v)^*\Big) - \frac{Z-a^n}{\varepsilon}\Big((h')^*_y - \frac{\tau}{\varepsilon}(h')^*_x\Big)\right] \tag{B.3b}$$
$$+ \frac{\Delta t}{2\gamma}\left(R^{hv,*} - \frac{\tau}{\varepsilon}R^{hu,*}\right) + \Delta t\Big(1-\frac{1}{2\gamma}\Big)\left(R^{hv,n} - \frac{\tau}{\varepsilon}R^{hu,n}\right)\Bigg\}.$$

Hereafter, we differentiate equations (B.3a) and (B.3b) with respect to x and y, respectively, and substitute the resulting equations into (B.2a). This yields the following elliptic equation for $(h')^{n+1}$:

$$\begin{aligned}
&(h')^{n+1} + \frac{(Z-a^*)(1-\alpha)}{\widetilde{K}_\tau}\big((h')^{n+1}_{xx} + (h')^{n+1}_{yy}\big)\\
&+ \frac{1-\alpha}{\widetilde{K}_\tau}\Big[(h')^{n+1}_x Z_x + (h')^{n+1}_y Z_y + \frac{\tau}{\varepsilon}\big((h')^{n+1}_y Z_x - (h')^{n+1}_x Z_y\big)\Big]\\
&= (h')^n + \frac{\Delta t}{2\gamma}R^{h',*} + \Delta t\Big(1-\frac{1}{2\gamma}\Big)R^{h',n} - (\Delta t-\tau)(1-\alpha)\Big[(\hat{h}u'+h'u)^*_x + (\hat{h}v'+h'v)^*_y\Big]\\
&- \frac{\tau(1-\alpha)}{K_\tau}\Bigg\{(\hat{h}u'+h'u)^n_x + (\hat{h}v'+h'v)^n_y + \frac{\tau}{\varepsilon}\Big[(\hat{h}v'+h'v)^n_x - (\hat{h}u'+h'u)^n_y\Big]\\
&+ \frac{\Delta t}{2\gamma}\Big[R^{hu,*}_x + R^{hv,*}_y + \frac{\tau}{\varepsilon}\big(R^{hv,*}_x - R^{hu,*}_y\big)\Big]\\
&+ \Delta t\Big(1-\frac{1}{2\gamma}\Big)\Big(R^{hu,n}_x + R^{hv,n}_y + \frac{\tau}{\varepsilon}(R^{hv,n}_x - R^{hu,n}_y)\Big)\Bigg\}\\
&- \frac{\tau(1-\alpha)(\Delta t-\tau)}{\varepsilon K_\tau}\Bigg\{\frac{1}{\varepsilon}\Big[(Z-a^n)\big((h')^*_{xx} + (h')^*_{yy}\big) + (h')^*_x Z_x + (h')^*_y Z_y\\
&+ \frac{\tau}{\varepsilon}\big((h')^*_y Z_x - (h')^*_x Z_y\big)\Big] + (\hat{h}v'+h'v)^*_x - (\hat{h}u'+h'u)^*_y\\
&- \frac{\tau}{\varepsilon}\Big[(\hat{h}u'+h'u)^*_x + (\hat{h}v'+h'v)^*_y\Big]\Bigg\}.
\end{aligned} \tag{B.4}$$

Finally, we proceed as in Section 3.4 and compute the nonstiff flux terms $R^{h',n}$, $R^{hu,n}$, $R^{hv,n}$ $R^{h',*}$, $R^{hu,*}$ and $R^{hv,*}$ in equations (B.3) and (B.4) using the CU numerical flux from Section 3.3 and discretize the spatial derivatives in (B.4) using the standard second-order central differences D_x

and D_y defined in (3.17). This results in

$$
\begin{aligned}
&\overline{(h')}_{j,k}^{n+1} + \frac{(Z_{j,k}-a^*)(1-\alpha)}{\widetilde{K}_\tau}\widetilde{\Delta}\,\overline{(h')}_{j,k}^{n+1}\\
&+\frac{1-\alpha}{\widetilde{K}_\tau}\Big[\Big(D_x-\frac{\tau}{\varepsilon}D_y\Big)Z_{j,k}D_x\,\overline{(h')}_{j,k}^{n+1}+\Big(D_y+\frac{\tau}{\varepsilon}D_x\Big)Z_{j,k}D_y\,\overline{(h')}_{j,k}^{n+1}\Big]\\
&=\overline{(h')}_{j,k}^{n}+\frac{\Delta t}{2\gamma}\mathcal{R}_{j,k}^{h',*}+\Delta t\Big(1-\frac{1}{2\gamma}\Big)\mathcal{R}_{j,k}^{h',n}\\
&-(\Delta t-\tau)(1-\alpha)\Big[D_x(\hat{h}u'+h'u)_{j,k}^{*}+D_y(\hat{h}v'+h'v)_{j,k}^{*}\Big]\\
&-\frac{\tau(1-\alpha)}{K_\tau}\Big\{D_x(\hat{h}u'+h'u)_{j,k}^{n}+D_y(\hat{h}v'+h'v)_{j,k}^{n}+\frac{\tau}{\varepsilon}\Big(D_x(\hat{h}v'+h'v)_{j,k}^{n}-D_y(\hat{h}u'+h'u)_{j,k}^{n}\Big)\\
&+\frac{\Delta t}{2\gamma}\Big[D_x\mathcal{R}_{j,k}^{hu,*}+D_y\mathcal{R}_{j,k}^{hv,*}+\frac{\tau}{\varepsilon}\big(D_x\mathcal{R}_{j,k}^{hv,*}-D_y\mathcal{R}_{j,k}^{hu,*}\big)\Big]\\
&\Delta t\Big(1-\frac{1}{2\gamma}\Big)\Big(D_x\mathcal{R}_{j,k}^{hu,n}+D_y\mathcal{R}_{j,k}^{hv,n}+\frac{\tau}{\varepsilon}\big(D_x\mathcal{R}_{j,k}^{hv,n}-D_y\mathcal{R}_{j,k}^{hu,n}\big)\Big)\Big\}\\
&-\frac{\tau(1-\alpha)(\Delta t-\tau)}{\varepsilon K_\tau}\Big\{\frac{1}{\varepsilon}\Big[(Z-a^n)\widetilde{\Delta}(h')_{j,k}^{*}+D_x(h')_{j,k}^{*}D_xZ_{j,k}+D_y(h')_{j,k}^{*}D_yZ_{j,k}\\
&+\frac{\tau}{\varepsilon}(D_x(h')_{j,k}^{*}D_xZ_{j,k}-D_x(h')_{j,k}^{*}D_yZ_{j,k})\Big]+D_x(\hat{h}v'+h'v)_{j,k}^{*}-D_y(\hat{h}u'+h'u)_{j,k}^{*}\\
&-\frac{\tau}{\varepsilon}\Big[D_x(\hat{h}u'+h'u)_{j,k}^{*}+D_y(\hat{h}v'+h'v)_{j,k}^{*}\Big]\Big\}.
\end{aligned}
\tag{B.5}
$$

Once the numerical solution $\overline{(h')}_{j,k}^{n+1}$ is obtained by solving the elliptic equation (B.5), we substitute it into equations (B.3a) and (B.3b) discretized using the standard central differences and obtain

$$
\begin{aligned}
\overline{(hu)}_{j,k}^{n+1}&=\hat{h}_{j,k}\hat{u}_{j,k}+\frac{1}{K_\tau}\Big\{\big(\hat{h}u'+h'u\big)_{j,k}^{n}+\frac{\tau}{\varepsilon}\big(\hat{h}v'+h'v\big)_{j,k}^{n}+\frac{(Z_{j,k}-a^*)\tau}{\varepsilon^2}\Big(D_x(h')_{j,k}^{n+1}+\frac{\tau}{\varepsilon}D_y(h')_{j,k}^{n+1}\Big)\\
&+\frac{\Delta t-\tau}{\varepsilon}\Big[\big(\hat{h}v'+h'v\big)_{j,k}^{*}-\frac{\tau}{\varepsilon}\big(\hat{h}u'+h'u\big)_{j,k}^{*}+\frac{Z_{j,k}-a^n}{\varepsilon}\Big(D_x(h')_{j,k}^{*}+\frac{\tau}{\varepsilon}D_y(h')_{j,k}^{*}\Big)\Big]\\
&+\frac{\Delta t}{2\gamma}\Big(\mathcal{R}_{j,k}^{hu,*}+\frac{\tau}{\varepsilon}\mathcal{R}_{j,k}^{hv,*}\Big)+\Delta t\Big(1-\frac{1}{2\gamma}\Big)\Big(\mathcal{R}_{j,k}^{hu,n}+\frac{\tau}{\varepsilon}\mathcal{R}_{j,k}^{hv,n}\Big)\Big\}
\end{aligned}
$$

and

$$
\begin{aligned}
\overline{(hv)}_{j,k}^{n+1}&=\hat{h}_{j,k}\hat{v}_{j,k}+\frac{1}{K_\tau}\Big\{\big(\hat{h}v'+h'v\big)_{j,k}^{n}-\frac{\tau}{\varepsilon}\big(\hat{h}u'+h'u\big)_{j,k}^{n}+\frac{(Z_{j,k}-a^*)\tau}{\varepsilon^2}\Big(D_y(h')_{j,k}^{n+1}-\frac{\tau}{\varepsilon}D_x(h')_{j,k}^{n+1}\Big)\\
&-\frac{\Delta t-\tau}{\varepsilon}\Big[\big(\hat{h}u'+h'u\big)_{j,k}^{*}+\frac{\tau}{\varepsilon}\big(\hat{h}v'+h'v\big)_{j,k}^{*}-\frac{Z_{j,k}-a^n}{\varepsilon}\Big(D_y(h')_{j,k}^{*}-\frac{\tau}{\varepsilon}D_x(h')_{j,k}^{*}\Big)\Big]\\
&+\frac{\Delta t}{2\gamma}\Big(\mathcal{R}_{j,k}^{hv,*}-\frac{\tau}{\varepsilon}\mathcal{R}_{j,k}^{hu,*}\Big)+\Delta t\Big(1-\frac{1}{2\gamma}\Big)\Big(\mathcal{R}_{j,k}^{hv,n}-\frac{\tau}{\varepsilon}\mathcal{R}_{j,k}^{hu,n}\Big)\Big\}.
\end{aligned}
$$

References

[1] U. M. ASCHER, S. J. RUUTH, AND R. J. SPITERI, *Implicit-explicit Runge-Kutta methods*

for time-dependent partial differential equations, Appl. Numer. Math., 25 (1997), pp. 151–167. Special issue on time integration (Amsterdam, 1996).

[2] E. Audusse, R. Klein, D. D. Nguyen, and S. Vater, *Preservation of the discrete geostrophic equilibrium in shallow-water flows*, in Finite volumes for complex applications VI. Problems & perspectives. Volume 1, 2, vol. 4 of Springer Proc. Math., Springer, Heidelberg, 2011, pp. 59–67.

[3] E. Audusse, R. Klein, and A. Owinoh, *Conservative discretization of Coriolis force in a finite volume framework*, J. Comput. Phys., 228 (2009), pp. 2934–2950.

[4] G. Bispen, K. R. Arun, M. Lukáčová-Medviďová, and S. Noelle, *IMEX large time step finite volume methods for low Froude number shallow water flows*, Commun. Comput. Phys., 16 (2014), pp. 307–347.

[5] G. Bispen, M. Lukáčová-Medviďová, and L. Yelash, *Asymptotic preserving IMEX finite volume schemes for low Mach number Euler equations with gravitation*, J. Comput. Phys., 335 (2017), pp. 222–248.

[6] N. Botta, R. Klein, S. Langenberg, and S. Lützenkirchen, *Well balanced finite volume methods for nearly hydrostatic flows*, J. Comput. Phys., 196 (2004), pp. 539–565.

[7] F. Bouchut, *Nonlinear stability of finite volume methods for hyperbolic conservation laws and well-balanced schemes for sources*, Frontiers in Mathematics, Birkhäuser Verlag, Basel, 2004.

[8] F. Bouchut, J. Le Sommer, and V. Zeitlin, *Frontal geostrophic adjustment and nonlinear wave phenomena in one-dimensional rotating shallow water. II. High-resolution numerical simulations*, J. Fluid Mech., 514 (2004), pp. 35–63.

[9] A. Chertock, M. Dudzinski, A. Kurganov, and M. Lukáčová-Medviďová, *Well-balanced schemes for the shallow water equations with Coriolis forces*, Numer. Math., 138 (2018), pp. 939–973.

[10] P. Degond and M. Tang, *All speed scheme for the low Mach number limit of the isentropic Euler equations*, Commun. Comput. Phys., 10 (2011), pp. 1–31.

[11] P. J. Dellar and R. Salmon, *Shallow water equations with a complete coriolis force and topography*, Phys. Fluids, 17 (2005), p. 106601.

[12] G. Dimarco, R. Loubère, and M.-H. Vignal, *Study of a new asymptotic preserving scheme for the Euler system in the low Mach number limit*, SIAM J. Sci. Comput., 39 (2017), pp. A2099–A2128.

[13] A. Duran, F. Marche, R. Turpault, and C. Berthon, *Asymptotic preserving scheme for the shallow water equations with source terms on unstructured meshes*, J. Comput. Phys., 287 (2015), pp. 184–206.

[14] J. Haack, S. Jin, and J.-G. Liu, *An all-speed asymptotic-preserving method for the isentropic Euler and Navier-Stokes equations*, Commun. Comput. Phys., 12 (2012), pp. 955–980.

[15] A. HARTEN, P. LAX, AND B. VAN LEER, *On upstream differencing and Godunov-type schemes for hyperbolic conservation laws*, SIAM Rev., 25 (1983), pp. 35–61.

[16] J. S. HESTHAVEN, *Numerical methods for conservation laws*, vol. 18 of Computational Science & Engineering, Society for Industrial and Applied Mathematics (SIAM), Philadelphia, PA, 2018. From analysis to algorithms.

[17] J. HU, S. JIN, AND Q. LI, *Asymptotic-preserving schemes for multiscale hyperbolic and kinetic equations*, in Handbook of numerical methods for hyperbolic problems, vol. 18 of Handb. Numer. Anal., Elsevier/North-Holland, Amsterdam, 2017, pp. 103–129.

[18] S. JIN, *Runge-Kutta methods for hyperbolic conservation laws with stiff relaxation terms*, J. Comput. Phys., 122 (1995), pp. 51–67.

[19] ——, *Efficient asymptotic-preserving (AP) schemes for some multiscale kinetic equations*, SIAM J. Sci. Comput., 21 (1999), pp. 441–454 (electronic).

[20] ——, *Asymptotic preserving (AP) schemes for multiscale kinetic and hyperbolic equations: a review*, Riv. Mat. Univ. Parma, 3 (2012), pp. 177–2016.

[21] R. KLEIN, *Scale-dependent models for atmospheric flows*, Annu. Rev. Fluid Mech., 42 (2010), pp. 249–274.

[22] A. C. KUO AND L. M. POLVANI, *Nonlinear geostrophic adjustment, cyclone/anticyclone asymmetry, and potential vorticity rearrangement*, Phys. Fluids, 12 (2000), pp. 1087–1100.

[23] A. KURGANOV, *Finite-volume schemes for shallow-water equations*, Acta Numer., 27 (2018), pp. 289–351.

[24] A. KURGANOV AND C.-T. LIN, *On the reduction of numerical dissipation in central-upwind schemes*, Commun. Comput. Phys., 2 (2007), pp. 141–163.

[25] A. KURGANOV, S. NOELLE, AND G. PETROVA, *Semidiscrete central-upwind schemes for hyperbolic conservation laws and Hamilton-Jacobi equations*, SIAM J. Sci. Comput., 23 (2001), pp. 707–740.

[26] A. KURGANOV AND G. PETROVA, *A second-order well-balanced positivity preserving central-upwind scheme for the saint-venant system*, Commun. Math. Sci., 5 (2007), pp. 133–160.

[27] A. KURGANOV, M. PRUGGER, AND T. WU, *Second-order fully discrete central-upwind scheme for two-dimensional hyperbolic systems of conservation laws*, SIAM J. Sci. Comput., 39 (2017), pp. A947–A965.

[28] A. KURGANOV AND E. TADMOR, *New high-resolution central schemes for nonlinear conservation laws and convection-diffusion equations*, J. Comput. Phys., 160 (2000), pp. 241–282.

[29] ——, *Solution of two-dimensional riemann problems for gas dynamics without riemann problem solvers*, Numer. Methods Partial Differential Equations, 18 (2002), pp. 584–608.

[30] R. LEVEQUE, *Finite volume methods for hyperbolic problems*, Cambridge Texts in Applied Mathematics, Cambridge University Press, Cambridge, 2002.

[31] K.-A. Lie and S. Noelle, *On the artificial compression method for second-order nonoscillatory central difference schemes for systems of conservation laws*, SIAM J. Sci. Comput., 24 (2003), pp. 1157–1174.

[32] X. Liu, A. Chertock, and A. Kurganov, *An asymptotic preserving scheme for the two-dimensional shallow water equations with Coriolis forces*, J. Comput. Phys., 391 (2019), pp. 259–279.

[33] M. Lukáčová-Medviďová, S. Noelle, and M. Kraft, *Well-balanced finite volume evolution Galerkin methods for the shallow water equations*, J. Comput. Phys., 221 (2007), pp. 122–147.

[34] A. Majda, *Introduction to PDEs and waves for the atmosphere and ocean*, vol. 9 of Courant Lecture Notes in Mathematics, New York University, Courant Institute of Mathematical Sciences, New York; American Mathematical Society, Providence, RI, 2003.

[35] H. Nessyahu and E. Tadmor, *Nonoscillatory central differencing for hyperbolic conservation laws*, J. Comput. Phys., 87 (1990), pp. 408–463.

[36] S. Noelle, G. Bispen, K. R. Arun, M. Lukáčová-Medviďová, and C.-D. Munz, *A weakly asymptotic preserving low Mach number scheme for the Euler equations of gas dynamics*, SIAM J. Sci. Comput., 36 (2014), pp. B989–B1024.

[37] J. Pedlosky, *Geophysical Fluid Dynamics*, Springer-Verlag, New York, 2nd ed., 1987.

[38] A. L. Stewart and P. J. Dellar, *Multilayer shallow water equations with complete Coriolis force. Part 1. Derivation on a non-traditional beta-plane*, J. Fluid Mech., 651 (2010), pp. 387–413.

[39] ——, *Two-layer shallow water equations with complete Coriolis force and topography*, in Progress in industrial mathematics at ECMI 2008, vol. 15 of Math. Ind., Springer, Heidelberg, 2010, pp. 1033–1038.

[40] P. K. Sweby, *High resolution schemes using flux limiters for hyperbolic conservation laws*, SIAM J. Numer. Anal., 21 (1984), pp. 995–1011.

[41] G. K. Vallis, *Atmospheric and Oceanic Fluid Dynamics: Fundamentals and Large-Scale Circulation*, Cambridge University Press, 2006.

[42] B. van Leer, *Towards the ultimate conservative difference scheme. V. A second-order sequel to Godunov's method*, J. Comput. Phys., 32 (1979), pp. 101–136.

[43] S. Vater and R. Klein, *A semi-implicit multiscale scheme for shallow water flows at low Froude number*, Commun. Appl. Math. Comput. Sci., 13 (2018), pp. 303–336.

[44] H. Zakerzadeh, *The RS-IMEX scheme for the rotating shallow water equations with the Coriolis force*, in Finite volumes for complex applications VIII—hyperbolic, elliptic and parabolic problems, vol. 200 of Springer Proc. Math. Stat., Springer, Cham, 2017, pp. 199–207.

[45] J. ZEIFANG, J. SCHÜTZ, K. KAISER, A. BECK, M. LUKÁČOVÁ-MEDVIĎOVÁ, AND S. NOELLE, *A novel full-Euler low Mach number IMEX splitting*, Commun. Comput. Phys., 27 (2020), pp. 292–320.

[46] V. ZEITLIN, *Geophysical Fluid Dynamics: Understanding (almost) Everything with Rotating Shallow Water Models*, Oxford University Press, Oxford, 2018.